Sedimentary Geology 364 (2018) 141–159

Contents lists available at ScienceDirect

Sedimentary Geology

journal homepage: www.elsevier.com/locate/sedgeo

# Detailed facies analysis of the Upper Cretaceous Tununk Shale Member, Henry Mountains Region, Utah: Implications for mudstone depositional models in epicontinental seas

Zhiyang Li *, Juergen Schieber

*Department of Earth and Atmospheric Sciences, Indiana University, 1001 East 10th Street Bloomington, Indiana 47405, United States*

ARTICLE INFO

*Article history:*
Received 10 October 2017
Received in revised form 12 December 2017
Accepted 13 December 2017
Available online 22 December 2017

Editor: Dr. B. Jones

*Keywords:*
Tununk Shale
Mudstone facies analysis
Mudstone depositional model
Storm-dominated shelf
Geostrophic current
Epicontinental seas

ABSTRACT

Lower-Middle Turonian strata of the Tununk Shale Member of the greater Mancos Shale were deposited along the western margin of the Cretaceous Western Interior Seaway during the Greenhorn second-order sea level cycle. In order to examine depositional controls on facies development in this mudstone-rich succession, this study delineates temporal and spatial relationships in a process-sedimentologic-based approach. The 3-dimensional expression of mudstone facies associations and their stratal architecture is assessed through a fully integrative physical and biologic characterization as exposed in outcrops in south-central Utah. Sedimentologic characteristics from the millimeter- to kilometer-scale are documented in order to fully address the complex nature of sediment transport mechanisms observed in this shelf muddy environment.

The resulting facies model developed from this characterization consists of a stack of four lithofacies packages including: 1) carbonate-bearing, silty and sandy mudstone (CSSM), 2) silt-bearing, calcareous mudstone (SCM), 3) carbonate-bearing, silty mudstone to muddy siltstone (CMS), and 4) non-calcareous, silty and sandy mudstone (SSM). Spatial and temporal variations in lithofacies type and sedimentary facies characteristics indicate that the depositional environments of the Tununk Shale shifted in response to the 2nd-order Greenhorn transgressive-regressive sea-level cycle. During this eustatic event, the Tununk shows a characteristic vertical shift from distal middle shelf to outer shelf (CSSM to SCM facies), then from outer shelf to inner shelf environment (SCM to CMS, and to SSM facies). Shifting depositional environments, as well as changes in dominant paleocurrent direction throughout this succession, indicate multiple source areas and transport mechanisms (i.e. longshore currents, offshore-directed underflows, storm reworking). This study provides a rare documentation of the Greenhorn cycle as exposed across the entire shelf setting. High-resolution mapping of genetically-related packages facilitate the development of process-based depositional models that can be utilized for lateral correlations into the equivalent foredeep strata of the Cretaceous Interior.



## 1. Introduction

Interpretation of the processes that govern transportation and deposition of mudstone-dominated systems is evolving rapidly due to new insights from experimental studies (e.g. Schieber et al., 2007; Schieber and Southard, 2009; Schieber, 2011) and a growing number of case studies that tap into new data sets that generated by intense exploration activity for unconventional hydrocarbon resources (e.g. Bohacs et al., 2005; Passey et al., 2010; Aplin and Macquaker, 2011; Wilson and Schieber, 2016; Knapp et al., 2017). Fine-grained sediments (i.e. all those composed mainly of particles smaller than 62.5 μm) have historically been considered as deposited through suspension fallout under mostly quiet conditions (e.g. Potter et al., 2005). However, recent flume experiments have shown that flocculated muds can be transported in bedload and form floccule ripples at flow velocities strong enough to facilitate bedload transport of sand (Schieber et al., 2007; Schieber and Southard, 2009; Schieber, 2011; Yawar and Schieber, 2017). Studies of modern muddy shelf sedimentation (Rine and Ginsburg, 1985; Kuehl et al., 1986; Nittrouer et al., 1986; Wright et al., 1988; Kineke et al., 1996; Allison et al., 2000; Traykovski et al., 2000; Liu et al., 2006; Dashtgard and MacEachern, 2016), as well as a growing number of facies analysis case studies of ancient mudstone successions, all point to the important role of bottom current dynamics (e.g. turbidity currents, storm-induced currents, and tidal currents, etc.) in transporting and depositing significant volumes of fluidized muds under energetic conditions across and along continental shelves (Bhattacharya and MacEachern, 2009; Plint, 2014; Wilson and Schieber, 2014; Harazim and McIlroy, 2015; Li et al., 2015; Wilson and Schieber, 2015; Schieber, 2016).

* Corresponding author.
*E-mail address:* zl29@iu.edu (Z. Li).

https://doi.org/10.1016/j.sedgeo.2017.12.015
0037-0738/

Despite recent advances in appreciating the complex and dynamic processes of mud deposition, there is still a general lack of depositional models that link various types of mudstone-dominated facies to different environments across continental shelves (Plint, 2014; Harazim and McIlroy, 2015; Wilson and Schieber, 2015; Birgenheier et al., 2017). This in part is due to the difficulty of outcrop study of these rocks, because they weather easily and tend to look rather homogenous and featureless, even though they may contain sedimentary features that can inform about underlying processes (Schieber, 1989, 1990; MacQuaker and Gawthorpe, 1993; Macquaker and Howell, 1999; Schieber, 1999; Lazar et al., 2015). To recognize, study, and analyze the small-scale (i.e. mm- to cm-scale) sedimentary features in mudstones is a time consuming undertaking, and this hurdle has historically hampered efforts to explore mudstones for their inherent variability in terms of sedimentary structures, bioturbation styles and depositional settings. In the literature this is reflected in mudstone successions that are largely undifferentiated and can be of substantial thickness, such as the Mancos Shale with a thickness in excess of 500 m (~ 1500 ft).

To better understand the nature and complex variability within the Mancos Shale, a thick shelf mudstone succession, a comprehensive depositional model based on high-resolution facies analysis is much needed. This study focuses on the extensive exposures (~200 m) of the Upper Cretaceous Tununk Shale Member of the greater Mancos Shale Formation. The primary goals of the present study are threefold. The first goal is to document different facies types and variations in facies characteristics (sedimentological and ichnological) within the Tununk Shale. The second goal is to understand the circulation pattern and dominant depositional processes within this ancient mud-dominated shelf system. The third goal is to propose a depositional model, which can be applied to predict the development and distribution of mudstone facies across shelf environments of the Tununk Shale and analogous muddy shelf environments.

## 2. Geological background and previous work

During the late Jurassic and Cretaceous, the geology of the western North America was largely controlled by the subduction of the Farallon place beneath the North American plate (Livaccari, 1991; DeCelles, 2004). The compressive forces associated with plate convergence, combined with conductive heating initiated by subduction, led to crustal thickening of orogenic belts such as the Sevier fold-thrust belt (Livaccari, 1991; DeCelles, 2004; Yonkee and Weil, 2015). The Sevier belt, consisting of a linear north–south belt of plutonism, volcanism, thrusting and folding, formed as a foreland-propagating (west to east) wedge during the Cretaceous (Kauffman, 1977; DeCelles, 2004; Yonkee and Weil, 2015). Flexural loading from thrust sheets produced an asymmetric foreland basin along and east of the active fold-thrust belt (DeCelles, 2004; Liu et al., 2011; Yonkee and Weil, 2015).

Global Greenhouse climate and elevated rates of sea-floor spreading persisted throughout the Late Cretaceous, resulting in a global eustatic highstand, which caused repeated flooding of the foreland basin (Kauffman, 1977, 1985; Kauffman and Caldwell, 1993; Miller et al., 2005; Hay, 2008; Haq, 2014). The resulting epicontinental sea, termed the Western Interior Seaway (WIS), connected the Gulf of Mexico and the Northern Boreal Sea during peak eustatic highstand in Middle Early Turonian time (Fig. 1). This epeiric seaway never exceeded more than a few hundred meters water depth (Weimer, 1984; Kauffman, 1985; Sageman and Arthur, 1994), but was up to 1500 km wide (Fig. 1). Palaeoenvironmental reconstructions of the WIS suggest that during most of the Late Cretaceous, circulation within the seaway was largely controlled by storms and waves that produced dominant southward-directed longshore currents and net sediment drift along the western margin of the seaway (Barron, 1989; Ericksen and Slingerland, 1990; Slingerland and Keen, 1999).

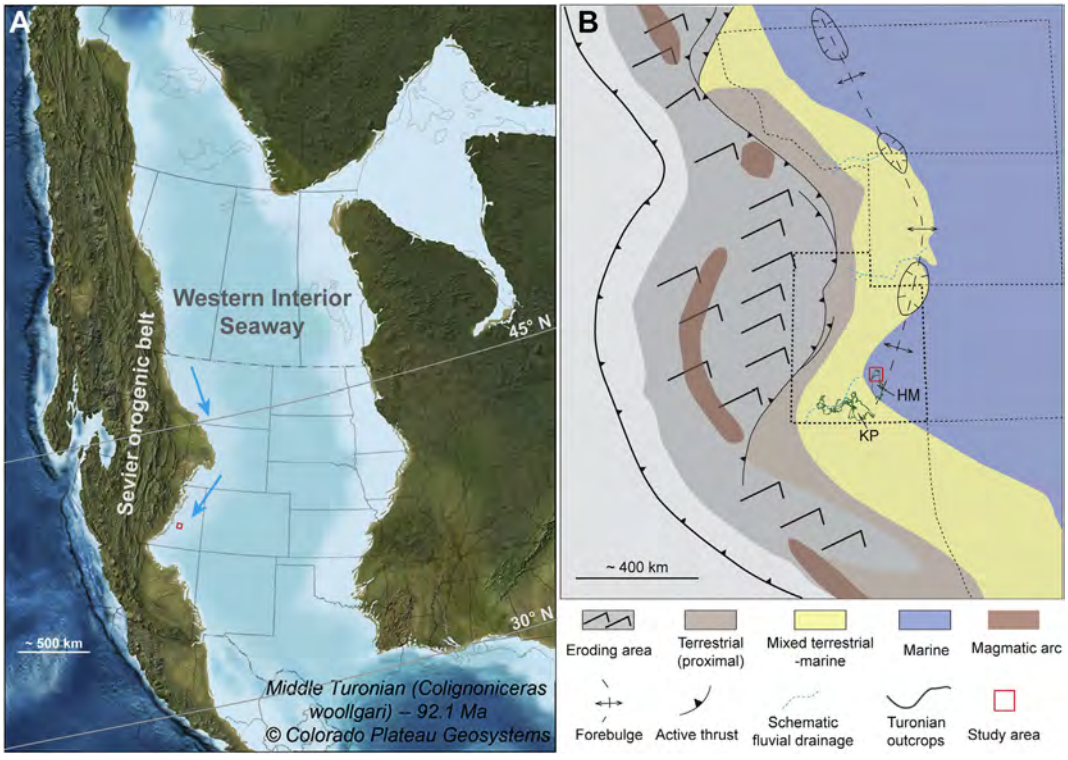


**Fig. 1.** A). Middle Turonian paleogeographic map showing extent of the Western Interior Seaway (Blakey, 2014). Dominant southward-directed longshore currents along the western margin of the seaway are indicated by blue arrows. Paleolatitudes are from Sageman and Arthur (1994). B). Paleogeographic reconstruction of the foreland basin of middle North America illustrating evolving topography (schematic), locations of active faults, general depositional environments, position of forebulge during Turonian time, and location of the study area (modified from Yonkee and Weil, 2015). HM: Henry Mountains region, KP: Kaiparowits Plateau. (For interpretation of the references to colour in this figure legend, the reader is referred to the web version of this article.)

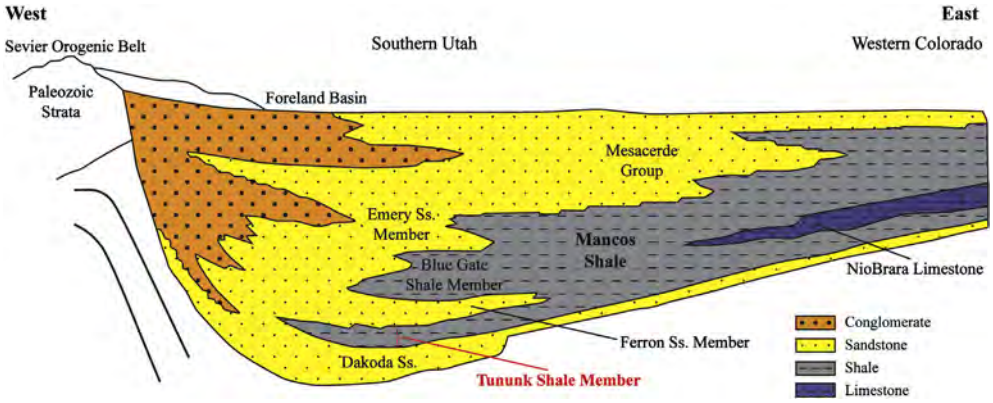


**Fig. 2.** Stratigraphic cross-section of Upper Cretaceous rocks from southern Utah to western Colorado (modified from Armstrong, 1968).

Late Cenomanian to Middle Turonian strata of the Tununk Shale Member of the Mancos Shale Formation were deposited along the western margin of the Western Interior Seaway (WIS) over a time span of about 2.5 million years (Zelt, 1985; Leithold, 1994). In response to sediments supplied from the Sevier orogenic belt to the west, the Upper Cretaceous sedimentary record along the western margin of the WIS shows multiple eastward prograding sandy clastic wedges that grade basinward into thick marine mudstone successions that are collectively known as the Mancos Shale (Fig. 2). A series of transgressive-regressive sequences primarily driven by second-order eustatic sea-level cycles have been identified in the deposits of the foredeep basin (Kauffman, 1985; Miall et al., 2008). In southern Utah, controlled by the Greenhorn transgressive-regressive sea-level cycle (Kauffman, 1977; Zelt, 1985; Leithold, 1994), the Tununk Shale overlies the underlying coarser nonmarine and paralic deposits of the Dakota Sandstone and grades upward into shallow marine and deltaic sandstones of the Ferron Sandstone Member (Fig. 3). The contact between the Tununk Shale and the underlying Dakota Sandstone is a regionally extensive disconformity characterized by an oyster coquina that formed during initial marine transgression (Gardner and Cross, 1994). The Tununk Shale was then deposited across these deposits of maximum transgression and during the gradual regression of the Greenhorn cycle (Fig. 3). The paleoshoreline during deposition of the Tununk Shale generally trended northeast-southwest (Fig. 1). The culmination of the regressive phase during the Greenhorn cycle is marked by deposition of the overlying Ferron Sandstone, which consists of three deltaic clastic wedges that were informally named the Vernal, Last Chance, and Notom delta systems (Bhattacharya and Tye, 2004).

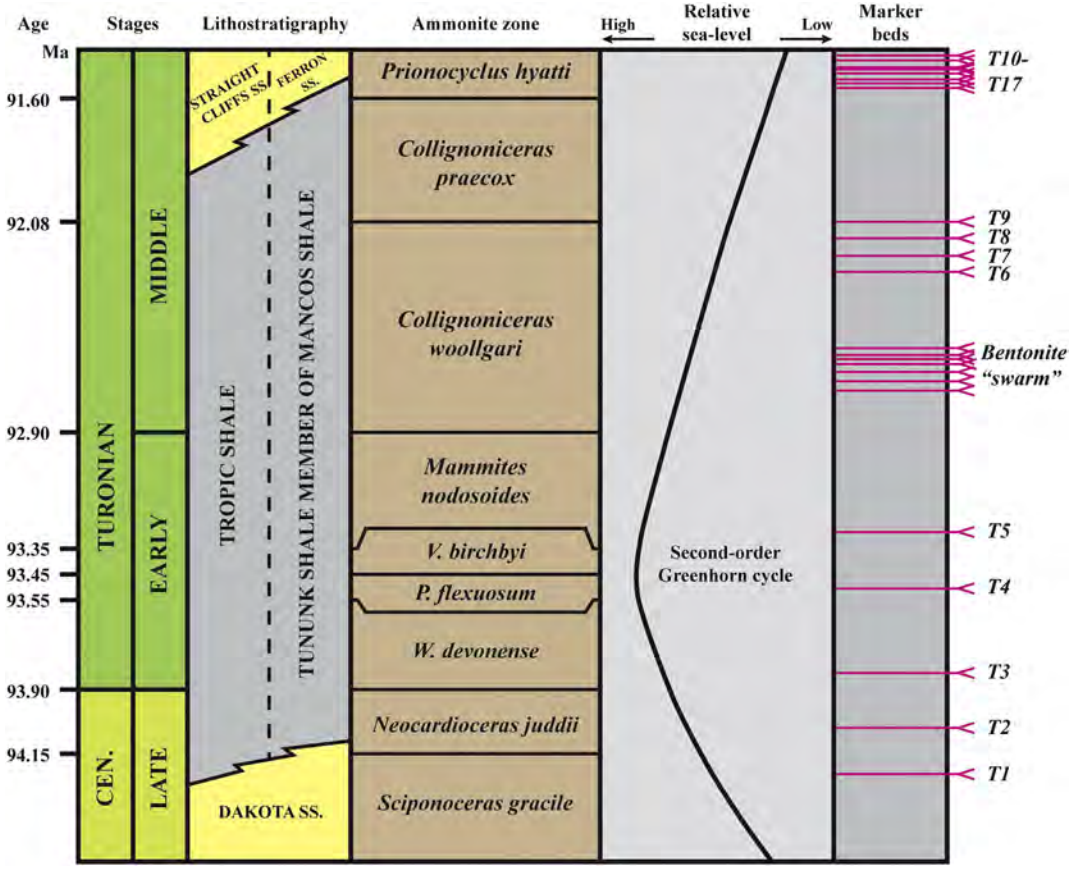


**Fig. 3.** Lower to middle Turonian stratigraphy in southern Utah (compiled from Zelt, 1985; Leithold, 1994; Leithold and Dean, 1998). Absolute dates are from Ogg et al. (2012).

In outcrop, the Tununk Shale is composed primarily of dark gray calcareous to non-calcareous mudstones with numerous thin silt- and sand-rich beds and volcanic ash beds (i.e. bentonites; Peterson et al., 1980; Zelt, 1985). Based on 17 traceable bentonite beds and biostratigraphic relations through an integrated surface to subsurface study, Zelt (1985) correlated the Tununk Shale in south-central Utah (Henry Mountains Region) with its lateral equivalent, the Tropic Shale in southern Utah (Kaiparowits Plateau) (Figs. 1 and 3). Within the stratigraphic framework developed by Zelt (1985), Leithold (1994) examined the Tropic and Tununk Shales in more detail through integrated analysis of textures (i.e., grain size) and mineralogy. Both the Tropic and Tununk Shales were interpreted to have been deposited in muddy prodeltaic environments based on the offshore prograding clinoform geometries as revealed by correlation of chronostratigraphic markers (i.e., bentonite beds) (Leithold, 1994; Sethi and Leithold, 1997; Leithold and Dean, 1998). Although in these prior studies general trends of sedimentary character were observed, at present there exists no facies model for this interval that would enable us to predict facies away from data control. Furthermore, the simple depositional models that were proposed previously for this succession have never been validated through systematic study of sedimentary facies in outcrop, and our study shows that they do not adequately capture the significant variability of mudstone facies in the Tununk Shale.

## 3. Methodology

In the current study, the Tununk Shale exposed in the Henry Mountains region in south-central Utah was examined to collect data for a comprehensive sedimentologic analysis. Three detailed stratigraphic sections of the Tununk Shale near Hanksville, Utah, oriented parallel to the paleoshoreline direction (NE to SW), were measured using a Jacob staff (1.5 m long) along a 30-km transect (Fig. 4). Due to the high susceptibility to weathering of these rocks, steep exposures were chosen and excavated where needed to reveal fresh rock for description and sample collection. For every 1.5 m interval determined by the Jacob staff, two small trenches (up to several tens of centimeters in both depth and length) were dug at the lower 1/3 and upper 1/3 locations to expose fresh surfaces. Within each section, relatively unweathered samples were collected at an average vertical spacing of 1 m (more closely spaced in some places). More than 500 samples, collected from three measured sections, were taken back to the laboratory, embedded in epoxy, and slabbed and polished for examination of small-scale sedimentary features and facies variability. Forty-one polished thin sections (20–25 μm thick) were made from selected samples to collect information on rock composition and textural attributes through petrographic and scanning electron microscope (SEM) analysis.

For each stratigraphic section, sedimentological data including lithology, grain-size, sedimentary features, bioturbation features, paleocurrent data, and amount and types of fossil fragments were documented. In the field, grain size variability was mainly determined by: 1) feeling and chewing rock samples to estimate silt versus clay (i.e. gritty versus smooth) content, and 2) variations in colour. The relative percentage of silt estimated by chewing essentially mirrors the quartz-silt content and serves as a reliable proxy for grain size in mudstones that can be related to overall depositional setting and relative sea-level change (Williams et al., 2001; Li et al., 2015). In the lab, grain-size assessment was further calibrated by semi-quantitatively comparing petrographic and SEM photomicrographs of selected samples at a range of magnifications.

A variety of sedimentary structures (such as abundance and continuity of laminae, grading, ripples, scours, etc.), and biogenic features (trace fossil types, bioturbation intensity) were documented. The Bioturbation Index (BI) of Taylor and Goldring (1993) was used to characterize the bioturbation intensity in these rocks, and terminology of MacEachern et al. (2007) was used to identify specific burrows types. An abundance of small-scale (sub-millimeter scale) and subtle sedimentologic and biologic features that are almost impossible to resolve even in fairly fresh or deeply trenched outcrops, became readily recognizable on polished slabs (Fig. 5). In addition, polished slabs were crucial to document BI accurately, especially in outcrops with minimal

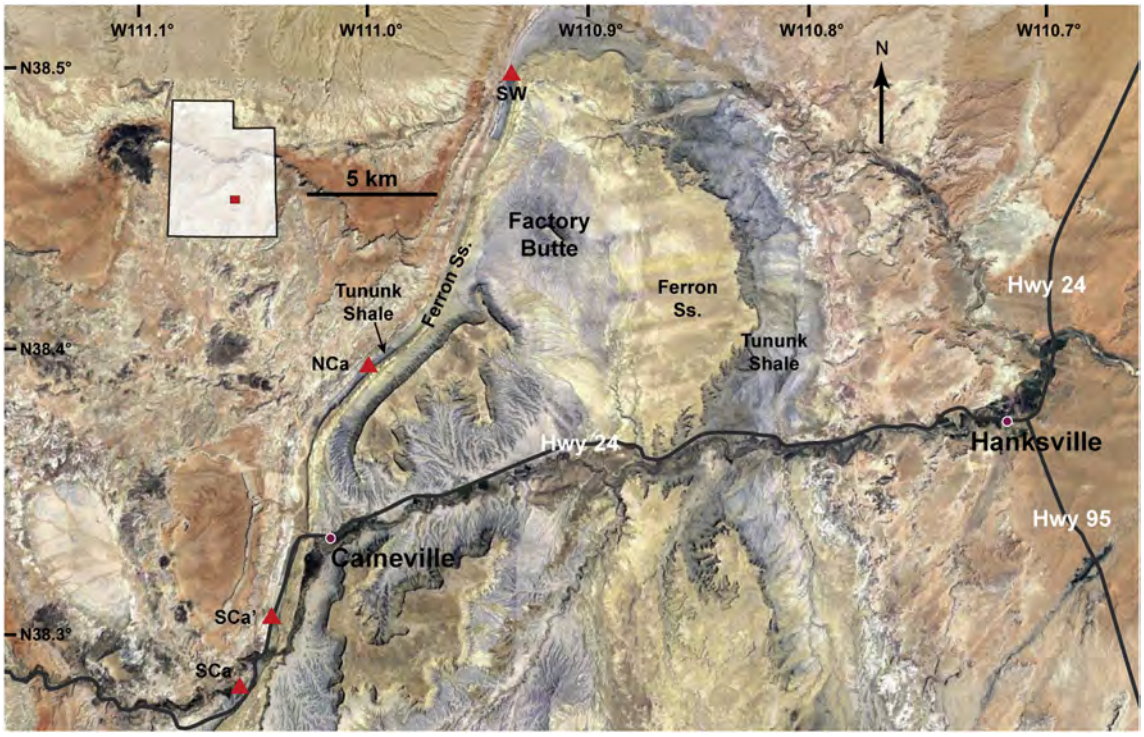


**Fig. 4.** Map showing outcrop belts of the Tununk Shale near Hanksville. Red triangles indicate locations of 3 stratigraphic sections measured in this study (SW: Salt Wash, NCa: North Caineville, and SCa: South Caineville). The section measured at SCa is a composite section consisting of two segments (SCa and SCa′). (For interpretation of the references to colour in this figure legend, the reader is referred to the web version of this article.)

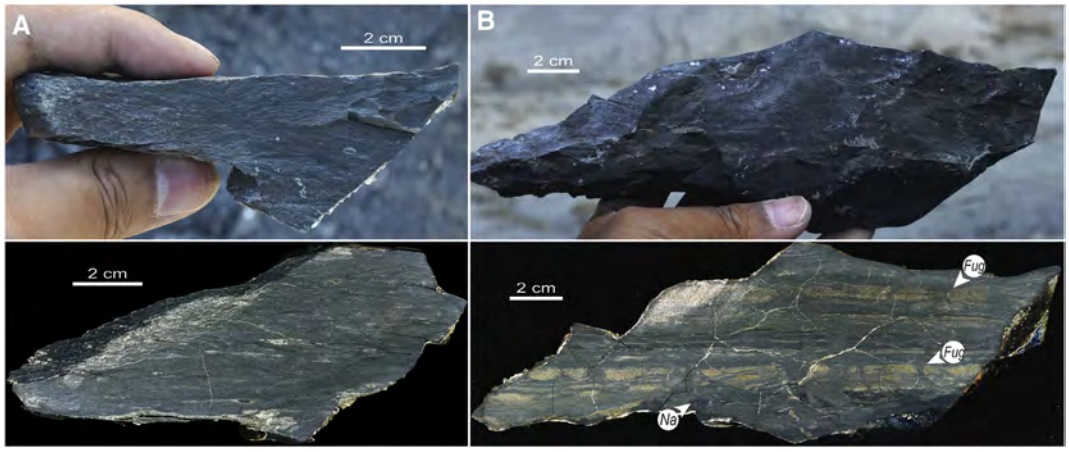


**Fig. 5.** Comparison between photos taken in the field (upper row) and scanned polished slabs (lower row) of same samples. Polishing is crucial to reveal abundant subtle sedimentary and biogenic features in these rocks and therefore is performed on all sample collected in this study. A) Highly bioturbated, carbonate-bearing, silty and sandy mudstone. B) Moderately bioturbated, silt-bearing, calcareous mudstone (Na: navichnia, *Fug*: *Fugichnia*).

lithologic contrast that were burrowed by small-sized (submillimeter to millimeter-scale) organisms (Fig. 5). In this study, sedimentary and biogenic features determined in the field and on polished slabs were merged to arrive at an as comprehensive as possible sedimentologic assessment of the exposed strata.

Paleocurrent data, including dip directions of ripple foresets and strike direction of wave ripple and combined-flow ripple crests were documented in situ at intervals in which primary sedimentary fabrics have not been significantly disrupted due to bioturbation, in order to support interpretation of sediment dispersal patterns and depositional settings across and along the shelf. A facies key that summarizes the various aspects of sedimentary and biogenic features documented in this study is shown in Fig. 6.

## 4. Facies description and interpretation

In the study area, the Tununk Shale gradually thins southward, with a total thickness ranging from 210 m at Salt Wash (SW) to 170 m at South Caineville (SCa) (Fig. 4). All three stratigraphic sections can be correlated with a series of regionally continuous bentonite beds (T3-T10 as suggested by Zelt, 1985; Leithold, 1994). Sedimentary facies characteristics in the Tununk Shale are illustrated for the section measured at SW (Fig. 6), but the same facies characteristics are also observed in the other measured sections.

Four lithofacies packages were recognized on the basis of observations made on polished slabs and petrographic thin sections. Upsection these include: (1) carbonate-bearing (< 30% carbonate), silty and sandy mudstone (CSSM), (2) silt-bearing, calcareous mudstone (SCM, >30% carbonate), (3) carbonate-bearing, silty mudstone to muddy siltstone (CMS), and (4) non-calcareous, silty and sandy mudstone (SSM). Each lithofacies type shows a wide range of bioturbation intensity, and three general categories were used for descriptive purposes. These categories are (1) "low", BI = 1–2, primary sedimentary features are preserved and can be easily identified; (2) "medium", BI = 3–4, primary sedimentary features are commonly disrupted and only remnant features are preserved; and (3) "high", BI = 5–6, primary sedimentary features are highly disrupted, and it is difficult to identify any distinct sedimentary features. In combination with four lithofacies types, a total of 12 combinations are possible. For example, SCMl represents silt-bearing, calcareous mudstone with low BI, where the lower case letters "l", "m", and "h" represent low, medium, and high BI, respectively. Among all possible combinations, CSSMl, SCMh, and CMSl are not observed in this study, and thus a total of 9 types of "shale microfacies" (sensu Schieber and Zimmerle, 1998) are recognized in the Tununk Shale.

### 4.1. Carbonate-bearing, silty and sandy mudstone (CSSM) facies package

The CSSM facies occurs directly above the Dakota-Tununk contact (Fig. 6), and shows silt to sand lamina to lamina-sets that range from <1 mm to several millimeters in thickness (Fig. 7). Identifiable sedimentary features in this facies, such as starved-ripple cross lamination (common) and a minor amount of wave ripple lamination, are commonly disrupted by burrows (Figs. 7 and 8). Silt to sand lamina-sets have sharp bases and pinch out laterally over a distance of a few centimeters (Fig. 8). Identifiable sedimentary features vary in abundance within the CSSM facies package, but generally become less abundant upsection (Fig. 6). Inoceramid shell fragments are dispersed throughout the CSSM facies (Fig. 8).

Within the CSSM facies, the CSSMm (BI = 3–4) and CSSMh (BI = 5) microfacies can be distinguished. Bioturbation in the CSSM facies is expressed through layer mixing and disruption of laminae (Figs. 7 and 8). Although characterized by an overall high BI, this facies shows low trace-fossil diversity. Typical trace fossil types include navichnia (sediment-swimmer traces), *Phycosiphon*, *Chondrites*, and rare *Planolites* (Fig. 8).

Silt- to sand-sized particles in the CSSM facies are dominated by quartz and feldspar from a detrital source, with a subordinate amount of biogenic carbonate particles such as planktonic foraminifera and fecal pellets (Fig. 9). The clay-dominated matrix is slightly calcareous due to the presence of coccoliths (Fig. 9). Upsection, this facies becomes more calcareous, and shows a gradual decrease in the relative amount of silt to sand-sized detrital grains.

#### 4.1.1. Interpretation

The commonly observed starved-ripple laminations with unimodally-dipping foresets in the CSSM facies could be produced by storm-induced offshore-directed bottom currents or by shore-parallel to shore-oblique geostrophic currents (Aigner and Reineck, 1982; Swift et al., 1986; Snedden et al., 1988; Leckie and Krystinik, 1989; Duke, 1990). The occasional presence of wavy laminae and wave-ripple lamination suggests that sedimentation was influenced by episodic storms. The widespread mottled texture and style of laminae disruption in this facies is suggestive of organisms "swimming" through a soft/soupy substrate (Lobza and Schieber, 1999) in an environment with comparatively low sedimentation rates. Small burrow size and very low trace-fossil diversity could be interpreted to indicate low oxygen availability (e.g. Ekdale and Mason, 1988; Savrda and Bottjer, 1991) and relate to relatively high sea-level during this time. Observations from modern shelf seas suggest, however, that even modest reductions of oxygen concentrations can already

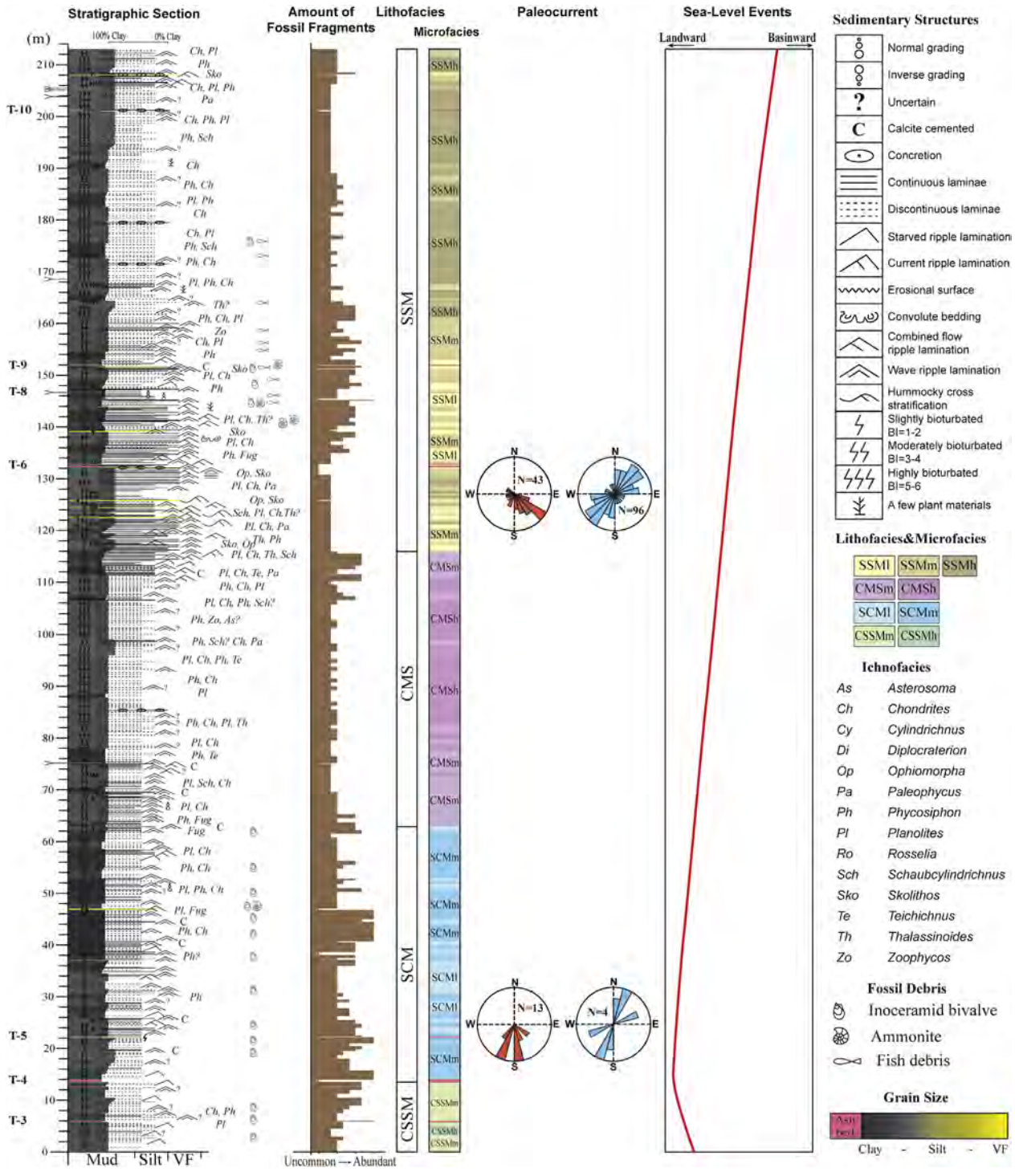


**Fig. 6.** The stratigraphic section of the Tununk Shale measured at Salt Wash (see Fig. 4 for location), with diagrams showing relative amount of fossil fragments, types of lithofacies and microfacies, paleocurrent data, and the second-order Greenhorn sea-level cycle.

dramatically affect the level of bioturbation in shelf muds (Dashtgard et al., 2015; Dashtgard and MacEachern, 2016).

The gradual decrease in the frequency of silt and sand laminae, and an upsection increase in the calcareous content in the CSSM facies suggests progressive deepening (less clastic dilution), related to the second-order Greenhorn transgression. Therefore, the CSSM facies probably records a gradual landward migration of the paleoshoreline and is interpreted to be primarily deposited in a distal middle-shelf to outer-shelf environment.

### 4.2. Silt-bearing, calcareous mudstone (SCM) facies package

The CSSM facies grades upward into the silt-bearing, calcareous mudstone (SCM) facies. Compared to the CSSM facies, the SCM facies shows more common and laterally continuous calcareous and silt laminae to lamina-sets ranging from <1 mm to several millimeters in thickness. Typical sedimentary structures present in the SCM facies include wave-ripple and combined-flow ripple lamination, and a small proportion of layers with normal grading, parallel lamination (both continuous

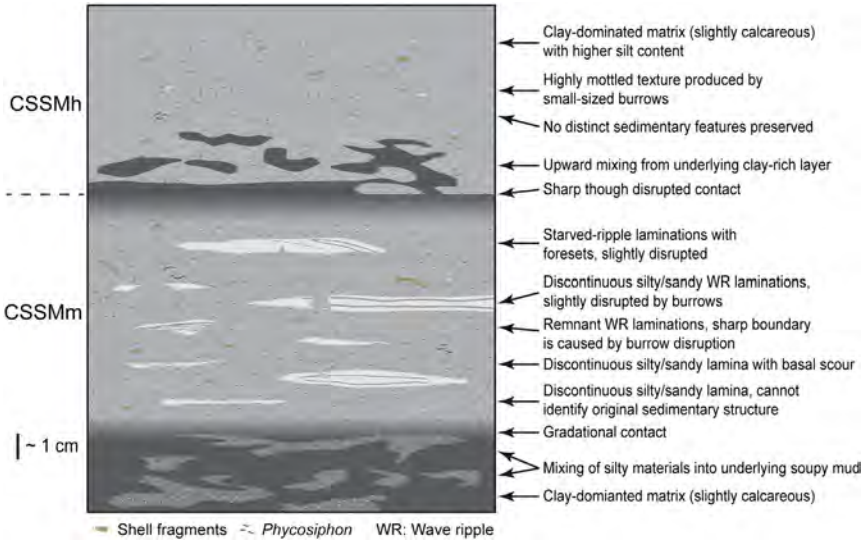


**Fig. 7.** Line drawings that summarize features observed in carbonate-bearing, silty and sandy mudstone (CSSM) facies.

and discontinuous), and starved-ripple lamination (Fig. 10). In the SCM facies, wave-ripple and combined-flow ripple lamination vary in both thickness and abundance, but generally become thicker and more common upsection (Figs. 6 and 11).

The SCM facies consists of two microfacies, SCMl (BI = 1–2) and SCMm (BI = 3–4), and shows a slight upward increase in both trace-fossil diversity and burrow size. The lower part of the SCM facies consists primarily of navichnia and *Phycosiphon*. Upsection these structures decrease in abundance and *Fugichnia* (escape structures), *Chondrites*, and *Planolites* (Figs. 5B and 11) become dominant.

Sub-millimeter to millimeter-scale lamina to lamina-sets in the SCM facies consist mostly of silt-/sand-sized calcareous particles with a minor fraction of detrital grains (Figs. 11B–E and 12A). Calcareous particles in this facies include planktonic foraminifera tests filled with early diagenetic calcite, fecal pellets, and shell fragments (Fig. 12). The fecal pellets, which are likely planktonic (Hattin, 1975; Honjo, 1976), consist almost exclusively of coccoliths (Fig. 12E and F) and impart a white-speckled appearance to polished slabs (Fig. 11B-C). In some intervals, many fecal pellets are concentrated along laminae and show preferential orientation (Fig. 12G and H). Abundant coccoliths are scattered throughout the matrix in the SCM facies.

Paleocurrent data derived from combined-flow ripple laminations indicate that the dominant direction of unidirectional flows is to the south-southwest. The dominant strike direction measured from 4 wave-ripple crests is north-east/south-west (Fig. 6).

#### 4.2.1. Interpretation

The lowermost portion of the SCM facies package is dominated by moderately bioturbated, highly calcareous mudstone (SCMm) facies. Distinct sedimentary features are rare, with exception of thin discontinuous laminae (Fig. 11A). Therefore, this interval is interpreted to record deposition during the highest relative sea level and record maximum transgression of the Greenhorn cycle. Upsection, an increase in the abundance and thickness of storm-generated sedimentary structures (e.g. wave-ripple and combined-flow ripple lamination), as well as a slight increase in burrow size and trace-fossil diversity, suggest increasing influence of storm events that likely are related to gradual shallowing (Figs. 6 and 11).

The high calcareous content of the SCM facies suggests a hemipelagic setting with very low clastic dilution. Sand-sized planktonic foraminifera are hydraulically equivalent to quartz silt (Oehmig, 1993), and finding them together in laminae suggests that both components were transported in bedload. Similarly, laminae composed of silt-/sand-sized particles such as fecal pellets (Figs. 11B–E and 12) also suggest bedload transport (Nowell et al., 1981; Minoura and Osaka, 1992).

The SCM facies appears to record an overall landward migration of the paleoshoreline relative to the underlying CSSM facies, and is interpreted to have been deposited primarily in an outer-shelf (hemipelagic) environment. Except for the very bottom of the SCM facies, which was deposited during the highest relative sea level, most of the SCM facies shows sedimentary features indicating storm-wave reworking. Therefore, the SCM facies was probably deposited around the average storm-wave base for silt (~70 m in the WIS as suggested by Plint, 2014).

The dominant direction of unidirectional flows in the SCM facies is to the south-southwest, which is almost parallel to the paleoshoreline orientation, indicating the dominant influence of shore-parallel geostrophic currents (Swift et al., 1986; Duke, 1990). Although the dominant direction of wave-ripple crests fits the orientation of the paleoshoreline well, the number of available measurements is rather small.

### 4.3. Carbonate-bearing, silty mudstone to muddy siltstone (CMS) facies package

The SCM facies grades upward into the carbonate-bearing, silty mudstone to muddy siltstone (CMS) facies. The CMS facies contains common silt lamina to lamina-sets with thickness ranging from a few millimeters to ~2 cm. Most primary sedimentary features in this facies are disrupted or absent due to pervasive bioturbation (Fig. 13). In intervals that are less bioturbated, silt lamina-sets dominantly show symmetrical forms, and therefore were interpreted as wave-ripple laminations (Fig. 14).

The CMS facies can be split into two microfacies, CMSm (BI = 3–4) and CMSh (BI = 5–6). Compared to the SCM facies, the CMS facies shows a distinct increase in both bioturbation intensity and diversity. Common types of trace fossils in this facies are those produced by deposit-feeding organisms such as *Phycosiphon*, *Chondrites*, *Planolites*, *Schaubcylindrichnus freyi*, *Zoophycos*, and *Thalassinoides* (Fig. 14).

Relative to the SCM facies, the CMS facies is characterized by significantly higher silt content and lower carbonate content. Types of calcareous particles include planktonic foraminifera, fecal pellets, and coccoliths (Fig. 15). Upsection, calcareous particles gradually decrease in abundance and are prone to suffer deformation by compaction between increasing amounts of harder silt grains such as quartz and feldspar (Fig. 15). Planktonic foraminifera tests in the CMS facies are more commonly filled with detritus (e.g. quartz, clay, pyrite) instead of diagenetic calcite (Fig. 15E and F).

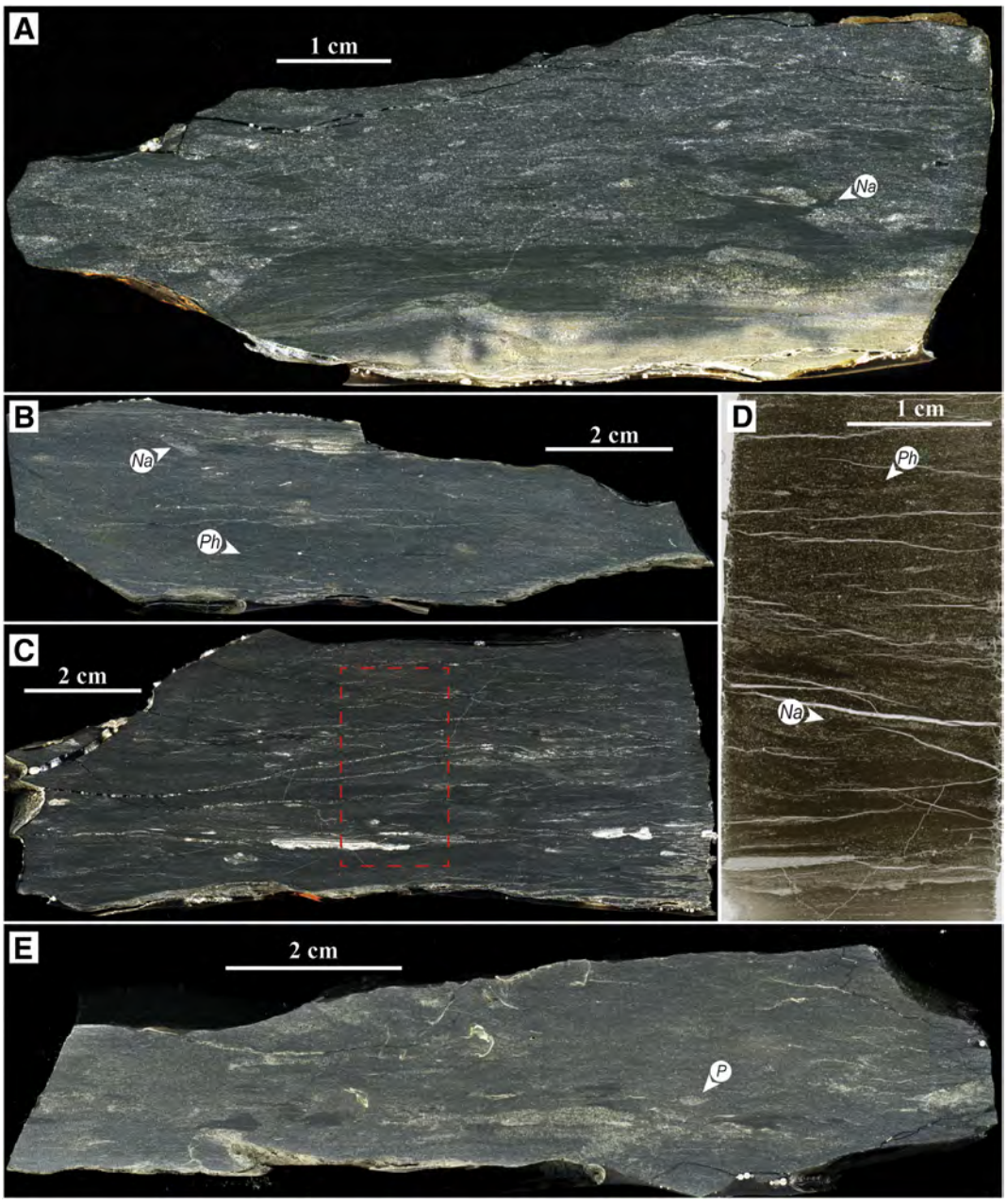


**Fig. 8.** Images of polished slabs and thin section scan of the CSSM facies. A) CSSMh facies with no distinct primary sedimentary feature. The upward mixing from underlying clay-rich layer is indicative of bioturbation in a soft/soupy substrate. B) CSSMm facies showing laterally discontinuous sandy wave-ripple laminations. C) CSSMm facies showing discontinuous silt/sand lamina to lamina-sets with scour bases and similar mixed layer fabrics as shown in A). D) Overview image of thin section made from the dashed area in C). Note sediment-swimming traces (*Na*: *navichnia*) and *Phycosiphon* (*Ph*) burrows. E) CSSMm facies showing silt/sand lamina-set with an asymmetrical and lenticular form (*P*: *Planolites*). Note foresets under the ripple crest, mixed layer fabrics, and common shell fragments. Samples of A) through E) are from stratigraphic lower to upper locations, and become more calcareous and less silty/sandy.

*4.3.1. Interpretation*

Although commonly disrupted, storm-generated sedimentary structures (mostly wave-ripple laminations) distinctly increase in abundance and thickness in the CMS facies, indicating influence of more frequent storm events and progressive shallowing. Nevertheless, the frequency of storm events is such that organisms are not prevented from pervasively disrupting the substrate in periods between these high energy events. Increases in both bioturbation diversity and burrow size in the CMS facies are thought to reflect higher oxygen levels and food availability, aspects that are both consistent with overall shallower water.

The greatly reduced calcareous content of the CMS facies probably reflects an increase of clastic dilution. Foraminifera tests filled with detritus instead of diagenetic calcite are suggestive of overall higher sedimentation rates that leave less time for early diagenetic calcite cementation of foram chambers, and imply a greater likelihood for deformation during compaction. The CMS facies records further basinward migration of the paleoshoreline and is interpreted to have been deposited in a middle-shelf environment with a higher degree of clastic dilution.

*4.4. Non-calcareous, silty and sandy mudstone (SSM) facies package*

The contact that separates the CMS facies from the overlying non-calcareous, silty and sandy mudstone (SSM) facies appears sharp and likely erosional. The SSM facies package shows a wide range of sedimentary

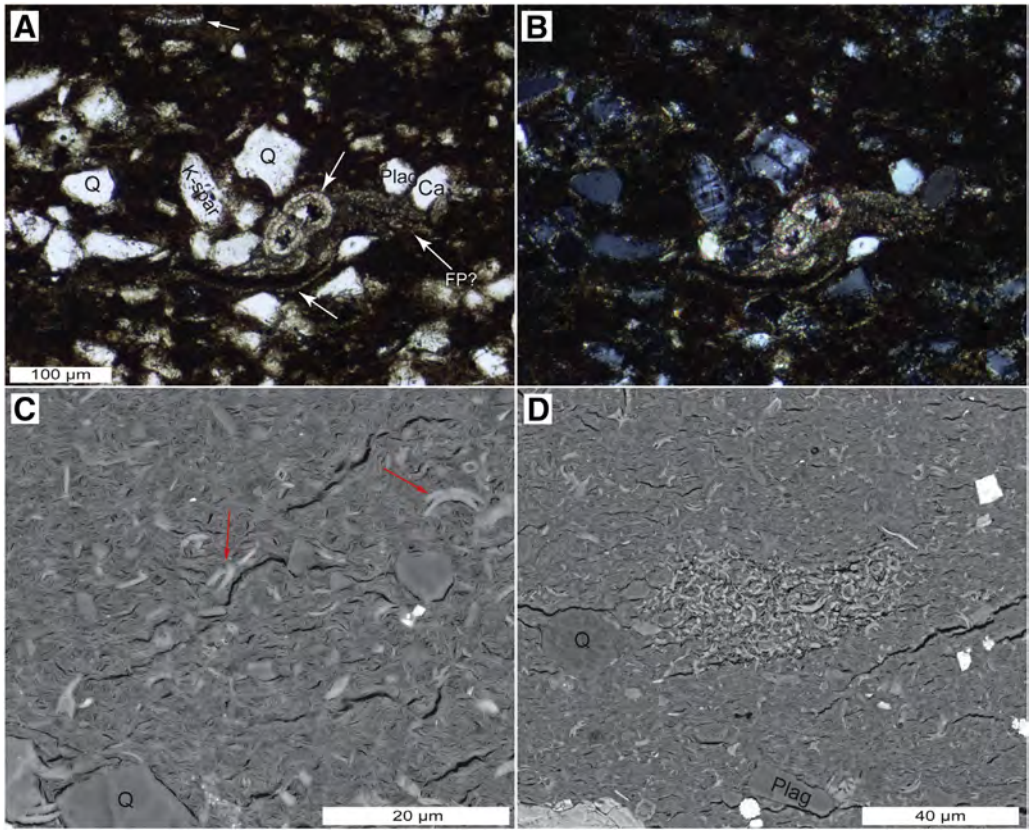


**Fig. 9.** A), B) Silt-/sand-sized particles in the CSSM facies consists of dominant amount of detrital grains such as quartz (Q) and feldspar (Plag: plagioclase, K-Spar: Potassium feldspar) and minor amount of calcareous particles (white arrows) such as foraminiferal tests and fecal pellet (FP?) (plane and cross-polarized light). C) Backscatter image showing the clay-dominated matrix in the CSSM facies consists dominant amount of clay (mostly montmorillonite), and small amount of coccoliths (red arrows), silt and pyrite. D) Backscatter image showing a fecal pellet in the matrix. The fecal pellet consists almost exclusively of coccoliths. (For interpretation of the references to colour in this figure legend, the reader is referred to the web version of this article.)

structures including common wave-ripple lamination, combined-flow ripple lamination, hummocky cross-stratification (HCS), a small amount of starved ripple and current ripple lamination, normal (and rare inverse) grading, and local soft sedimentary deformation (Figs. 16 and 17). Most silt/sand lamina to lamina-sets in this facies are sharp-based and range from a few millimeters to several centimeters in thickness, although a few sandstone beds showing HCS were found to be as thick as 14 cm in outcrop.

(The SSM facies shows a wide range of bioturbation intensity and contains three microfacies, SSMl (BI = 0–2), SSMm (BI = 3–4), and

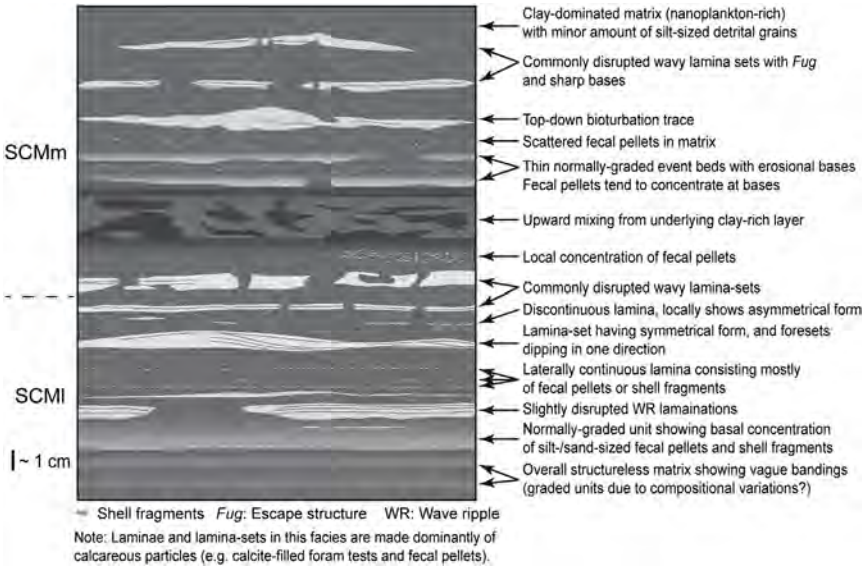


**Fig. 10.** Line drawings that summarize features observed in silt-bearing, calcareous mudstone (SCM) facies. Laminae and lamina-sets in this facies consist dominantly of calcareous particles such as calcite-filled foram tests and fecal pellets.

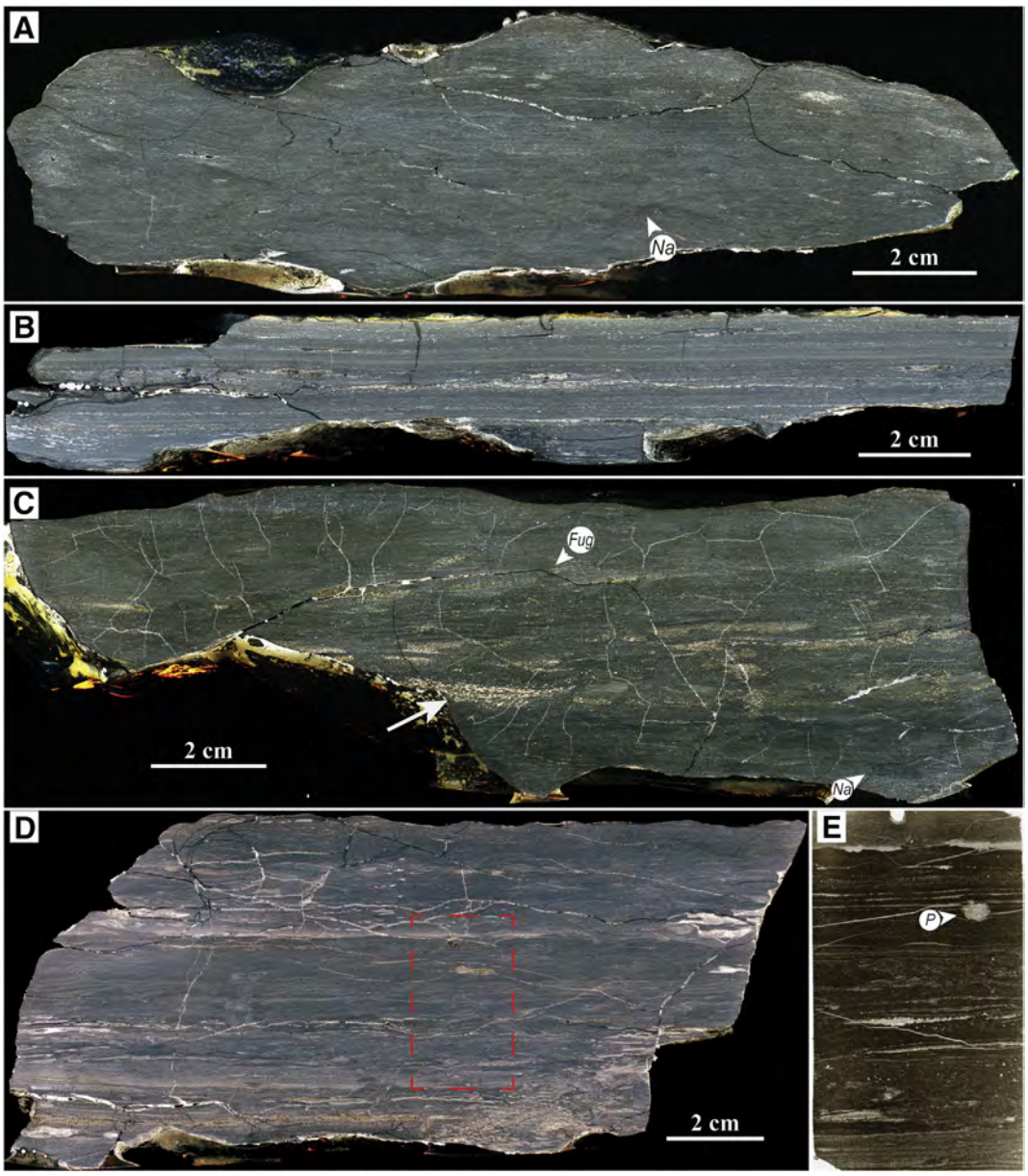


**Fig. 11.** Images of polished slabs and thin section scan of the SCM facies. A) SCMm facies showing mottled texture mostly due to navichnia (sediment-swimmer traces) and rare discontinuous silt laminae. B) SCMl facies showing common parallel to wavy laminae made dominantly by calcareous particles such as planktonic foraminifera tests, fecal pellets (white specks), and common fossil fragments. C) SCMm facies showing commonly disrupted laminae to lamina-sets with wavy/symmetrical crests (*Na*: *navichnia*, *Fug*: *Fugichnia*). Note prevalence and local concentration (white arrow) of fecal pellets on this slab. D) SCMl facies showing mixed layer fabrics, calcareous lamina to lamina-sets, and multiple small normally graded units (reflected by less concentration of silt/sand-sized calcareous particles upward). E) Overview image of thin section made from the dashed area in D) (*P*: *Planolites*). Width of image E) is 2.1 cm. Note common laminae (a few show symmetrical crest and normal grading) with sharp (erosional) basal contacts. Samples of A) through D) are from stratigraphic lower to upper locations, and show more common and thicker laminae and lamina-sets upward.

SSMh BI = 5–6). In addition to common ichnogenera such as *Phycosiphon*, *Chondrites*, *Planolites*, *Schaubcylindrichnus freyi*, *Teichichnus*, and *Thalassinoides*, the SSM facies locally shows a slight increase in the abundance of dwelling structures, including *Skolithos* and *Ophiomorpha* (Fig. 6).

Paleocurrent data measured from current ripple and combined-flow ripple laminations indicate that the dominant direction of unidirectional flows in the SSM facies is to the south-east, with a minor component to the south-southwest. The dominant strike direction measured from crests of wave ripple and combined-flow ripple is north-east/south-west (Fig. 6).

*4.4.1. Interpretation*

In the SSM facies, variations in abundance and dominance of certain types of sedimentary features, as well as bioturbation intensity, indicate significant changes in magnitude and frequency of depositional events (mostly storms). Relatively low bioturbation intensity, combined with a significant amount of storm-generated sedimentary structures and scours (SSMl microfacies) indicates repeated erosion and deposition resulting from high frequency storm events at relatively shallow water depth (Fig. 16). Localized soft sedimentary deformation may indicate liquefaction of surficial sediment by storm-wave loading (Owen and Moretti, 2011; Liu et al., 2017). The more bioturbated microfacies (SSMm and SSMh) reflect a decrease in the frequency and magnitude of storm events (Figs. 16 and 17). When compared to the CMS facies, the SSM facies appears to records further regression during the Greenhorn cycle and is interpreted to have been deposited in a storm-dominated inner shelf to lower shoreface environment.

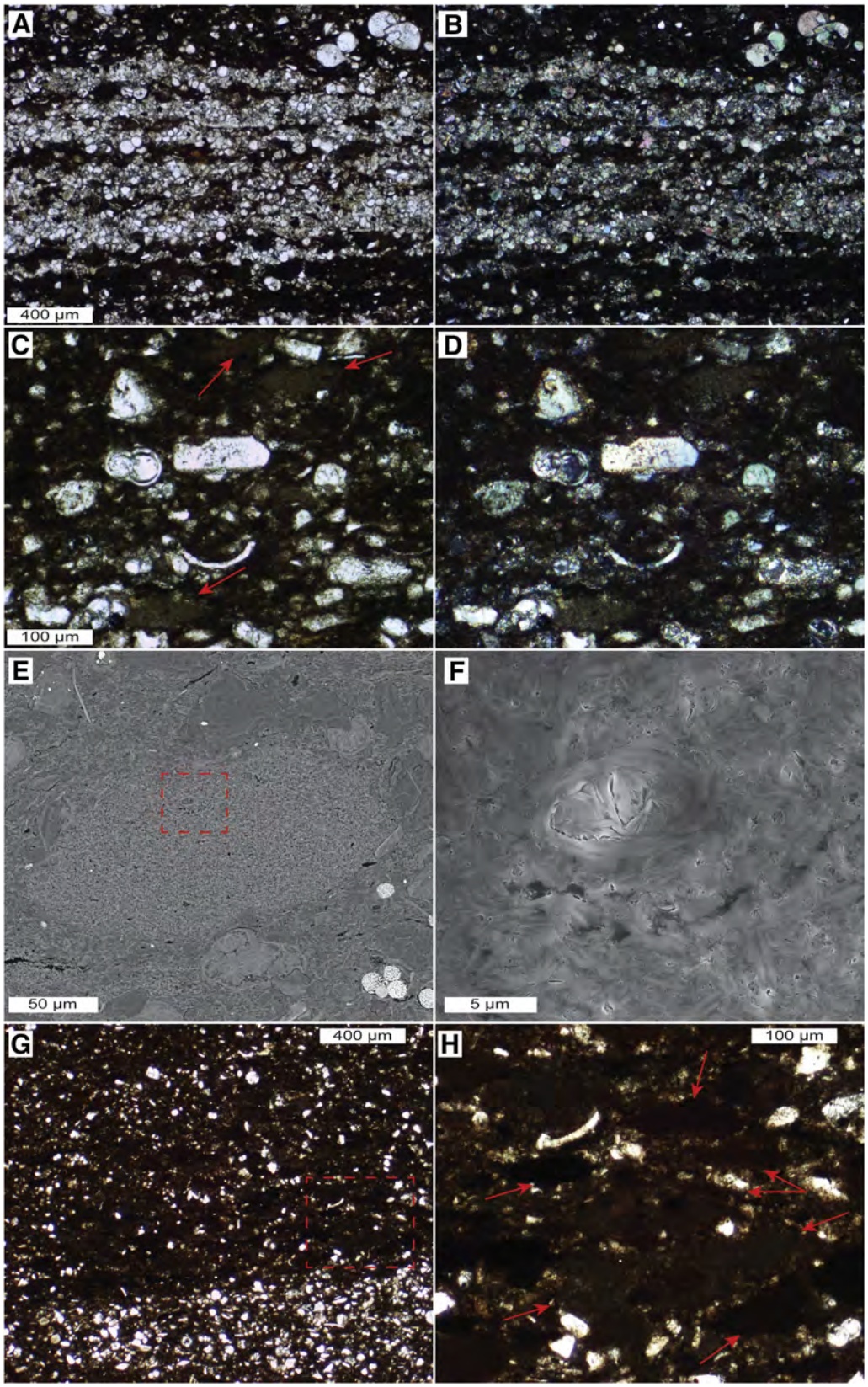


**Fig. 12.** A), B) Photomicrographs (plane and cross-polarized light) showing wavy lamina-set consisting dominantly silt/sand-sized planktonic foraminifera tests filled with calcite. C), D) Photomicrographs (plane and cross-polarized light) showing common silt/sand-sized calcareous particles including planktonic foraminifera tests, shell fragments, and fecal pellets (red arrows) in calcareous, clay-dominated matrix. E) Backscatter image showing a fine sand-sized (~200 μm in length) fecal pellet. F) Closer view of the dashed area in E) showing the fecal pellet is composed exclusively of coccoliths (secondary electron image). G) Photomicrograph showing a wavy lamina and its overlying layer (from an area in Fig. 11E, plane light). H) Closer view (plane light) of the dashed are in G). Abundant fecal pellets (red arrows) are present and show preferential orientation. All fecal pellets comprise dominantly coccoliths. Some fecal pellets contain a small amount of amorphous organic matter and clay-like particles (suggested by SEM examinations), and therefore exhibit dark brownish colour. (For interpretation of the references to colour in this figure legend, the reader is referred to the web version of this article.)

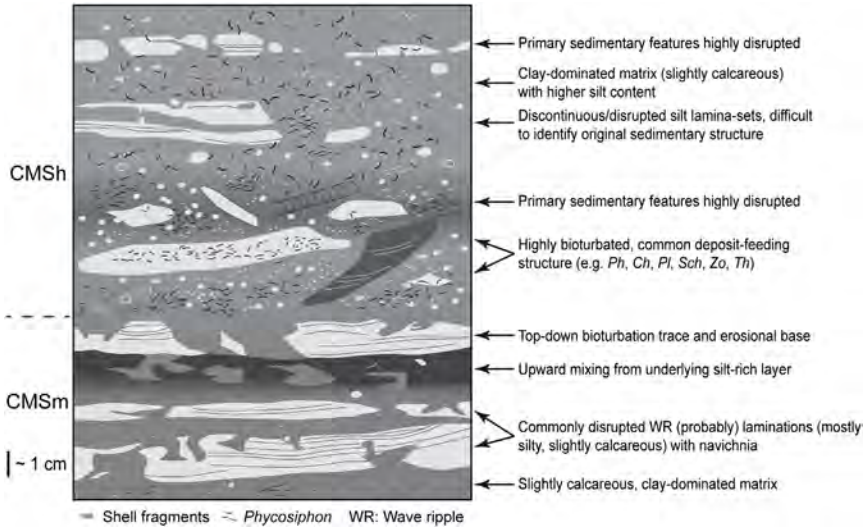


**Fig. 13.** Line drawings that summarize features observed in carbonate-bearing, silty mudstone to muddy siltstone (CMS) facies.

Unidirectional flows in the SSM facies show a dominant direction to the south-east, and a minor component to the south-southwest, flow directions which are perpendicular (offshore) and parallel (along-shore) to the paleoshoreline, respectively (Fig. 6). The dominant offshore-directed flows are interpreted as the result of downwelling currents produced by coastal sea-level set up during storms (Leckie and Krystinik, 1989; Duke, 1990). The subordinate component of alongshore-directed flows probably reflects longshore currents of lesser magnitude. The dominant direction of oscillatory storm surges inferred from the orientation of wave-ripple crests is largely perpendicular to the paleoshoreline (Fig. 6), consistent with the wave-refraction pattern in nearshore environments (Komar, 1998).

## 5. Discussion

### 5.1. Paleogeography during the deposition of the Tununk Shale

During the maximum transgression of the Greenhorn cycle, the study area was located approximately 110 km offshore (Fig. 18A). The transition from the underlying CSSM facies to the SCM facies (slightly above T4 in Fig. 6) marks the greatest water depth and minimal clastic dilution during deposition of the entire Tununk Shale. The lacuna depicted in Fig. 18A was persistently developed as a submarine unconformity from late Cenomanian to middle Turonian due to uplift of an intra-basinal culmination (named "Vernal High" in Ryer and Lovekin, 1986). The uplift produced a shoal area that was subject to constant

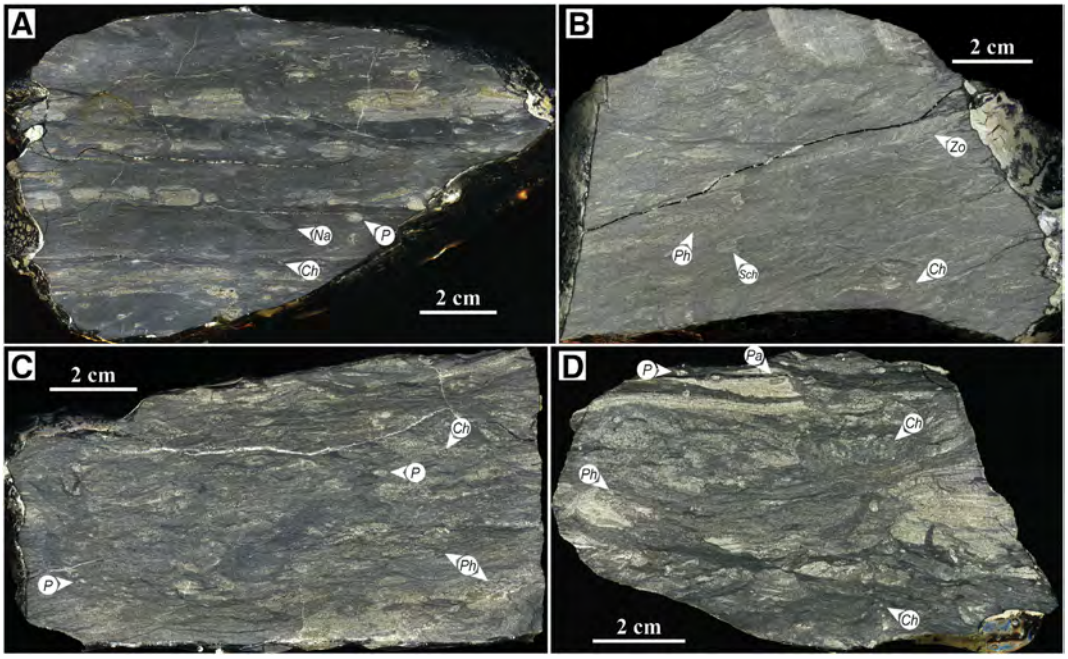


**Fig. 14.** Images of polished slabs of the CMS facies. A) and D): CMSm facies. B) and C): CMSh facies. Samples of A) through D) are from stratigraphic lower to upper locations, and become less calcareous and siltier. Although pervasively disrupted, remnant silt lamina to lamina-sets at certain intervals dominantly show symmetrical forms and are identified as wave-ripple laminations. Trace-fossil abbreviations include: *Chondrites* (*Ch*), *Planolites* (*Pl*), *navichnia* (*Na*), *Phycosiphon* (*Ph*), *Schaubcylindrichnus freyi* (*Sch*), and *Zoophycos* (*Zo*).

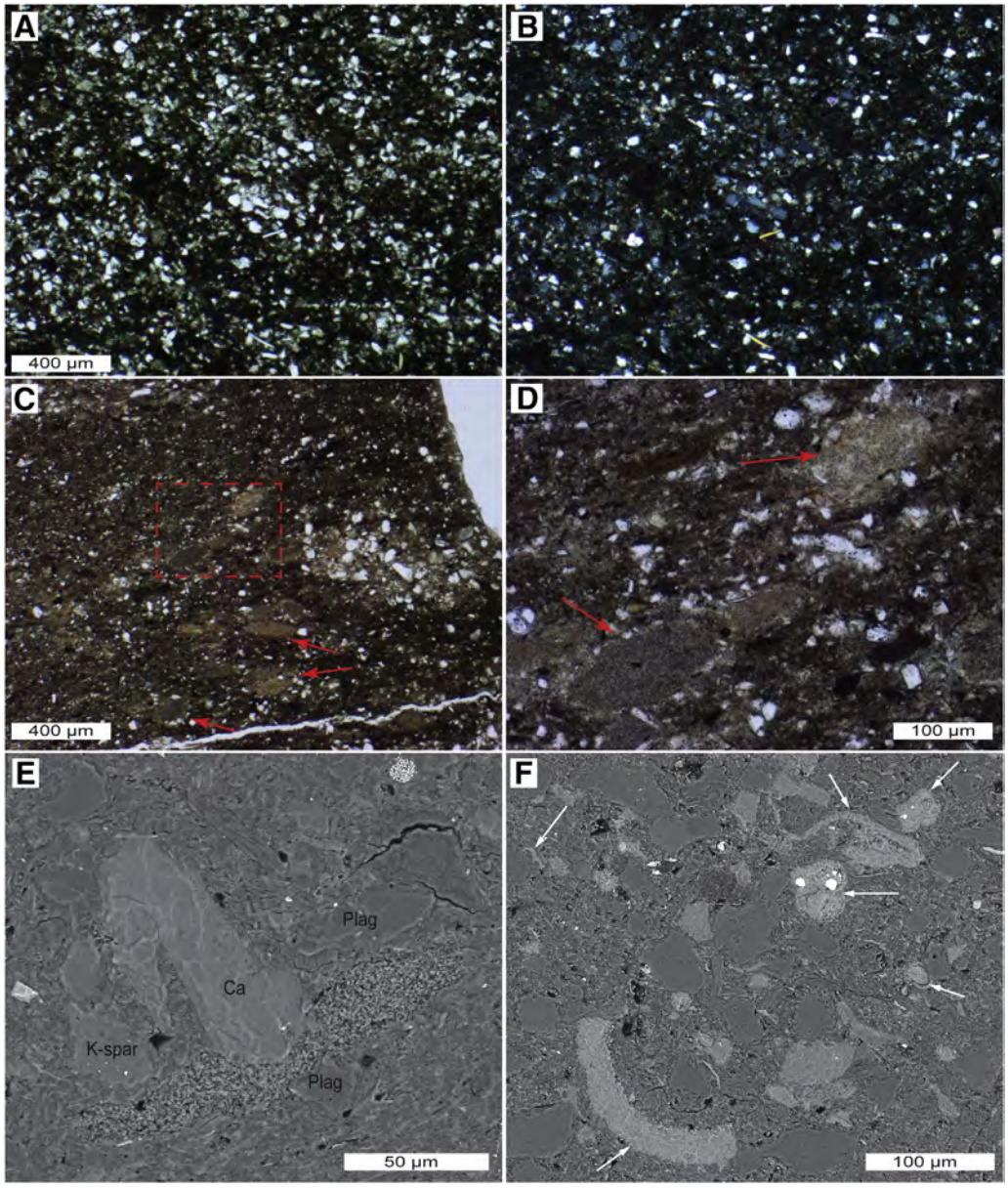


**Fig. 15.** A), B) Photomicrographs (plane and cross-polarized light) showing highly bioturbated texture in the CMS facies. Note distinctly decrease in the amount of calcareous particles and increase in the amount of silt-sized detrital particles (e.g. quartz, feldspar, mica). C) Photomicrograph (plane light) showing common presence of fecal pellets (red arrows) and bioturbated texture. Note a small silt-filled burrow on the middle right of the image. The inclined fecal pellets in the dashed box are due to texture disruption related to an inclined clay-filled burrow. D) Closer view of the dashed area in C) showing inclined fecal pellets (red arrows, plane light). E) Overview of an area showing a fecal pellet deformed by surrounding calcite (Ca) and feldspars. F) Overview of an area showing common broken and compacted foraminifera tests (white arrows). E) and F) are both backscatter images. (For interpretation of the references to colour in this figure legend, the reader is referred to the web version of this article.)

reworking and erosion of the bottom by wave-induced currents (Ryer and Lovekin, 1986).

During the subsequent regression of the Greenhorn cycle, the SCM grades upward into the CMS facies, reflecting an overall shallowing and increasing clastic dilution. By *Collignoniceras woollgari* time, the rise of the Vernal high gradually slowed, leading to a decrease in the extent of the area of nondeposition/erosion (Fig. 18B). During this time, the CMS facies gave way to the SSM facies in our study area. The lower sand-rich interval of the SSM facies (from ~115 m to T6 in Fig. 6) can be correlated to the Coon Spring Sandstone in northeastern Utah (Fig. 18B), a shelf sandstone as interpreted by Molenaar and Cobban (1991). The highly bioturbated Coon Spring Sandstone onlaps the Vernal high unconformity (lacuna) to the north, and shows a general thinning and fining trend towards the south (Fig. 18B). Molenaar and Cobban (1991) suggest that the Coon Spring Sandstone was at least partially formed by reworking of the Dakota Sandstone deposited on the Vernal High to the north.

By *Prionocyclus hyatti* time, the late stage of deposition of the Tununk Shale, the shoreline continued to migrate basinward. The northeastward progradation of the Ferron Notom delta (Gardner and Cross, 1994; Bhattacharya and Tye, 2004) forced further rapid basinward migration of the shoreline in our study area (Fig. 18C). This time period also coincides with the onset of the Last Chance and Vernal delta deposition in central and northeastern Utah, respectively (Fig. 18C). By this time, the Vernal area was no longer an area of uplift or erosion.

### 5.2. Implications from paleocurrent data

The dominant direction of sediment transport suggested by paleocurrent data has important implications for the interpretation of

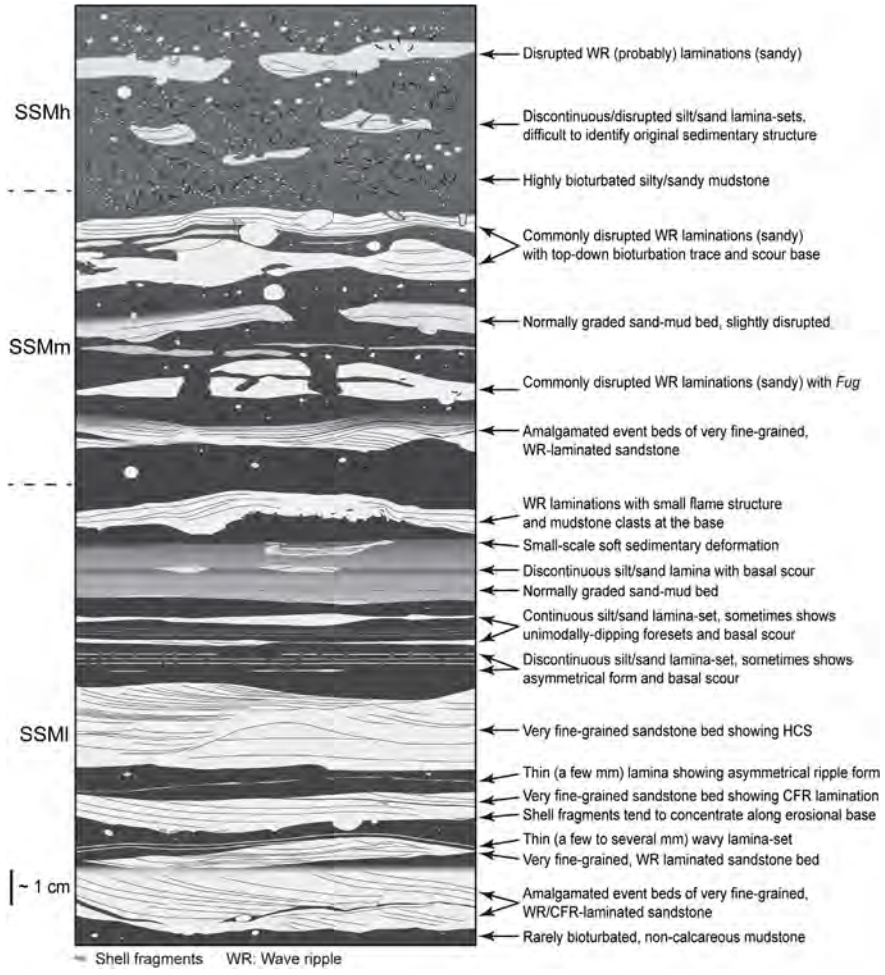


**Fig. 16.** Line drawings that summarize features observed in non-calcareous, silty to sandy mudstone (SSM) facies.

depositional environments. On a storm-dominated shelf, offshore-directed flows are inferred to be generated in response to hydraulic pressure that is generated by pile-up of water against the coast by winds (coastal set-up or storm surge) during storms (Swift et al., 1986; Duke, 1990). These offshore-directed bottom currents are then deflected by the Coriolis force, gradually changing these flows into shore-oblique and then shore-parallel geostrophic currents.

In the inner-shelf environments, due to the combined effects of the offshore-directed component of unidirectional flow (shore-oblique) and the storm/wave-generated oscillatory motion, bottom shear stress on the offshore stroke of waves is significantly increased, producing deposits with dominantly offshore-directed paleocurrent indicators (Leckie and Krystinik, 1989; Duke, 1990). At greater water depth (middle- to outer-shelf environments), storm-induced oscillatory motions commonly are much weaker compared to the geostrophic currents. As a result, paleocurrent data indicating dominant shore-parallel sediment transport may be more preferentially recorded in middle to outer-shelf deposits (Duke, 1990), a pattern that is also observed in this study. Paleocurrent data from the SCM and SSM facies indicate dominant direction of sediment transport alongshore and offshore, respectively, consistent with interpretations of depositional environments for these two facies (Fig. 6). However, it is important to note that paleocurrent data from the SSM facies contain a minor shore-parallel component to the south-southwest (Fig. 6), suggesting that geostrophic flows were still active processes that dispersed sediments in relatively high-energy settings, but unlikely to be reflected in the sedimentary record due to low preservation potential (Leckie and Krystinik, 1989). Therefore, the relatively weak but more sustained shore-parallel geostrophic currents play an important role in transporting sediments along a storm-dominated shelf, whereas the stronger but relatively short-lived offshore-directed currents, especially when aided by storm-generated oscillatory flows, are more capable of transporting sediments across the shelf.

### 5.3. A depositional model of shelf mudstones in epicontinental seas

Detailed analysis of the sedimentary facies characteristics indicate that the Tununk Shale was deposited as an offshore mud blanket on a storm-dominated shelf. Both paleogeography and paleocurrent data from the Tununk Shale indicate that sediment supply for the Tununk Shale dominantly came from north of the study area and was carried southward by longshore-currents (Fig. 19). The sediment supply of the Tununk Shale was derived from multiple sources. These include significant amounts of clastic sediments derived from the Sevier orogenic belt, primary productivity (e.g. foraminifera tests, fecal pellets and coccoliths), and possibly from erosion of previously deposited marine shales in the area of the Vernal High (Ryer and Lovekin, 1986). Upsection changes in Tununk lithofacies were dominantly caused by changing clastic dilution associated with relative sea-level changes during the second-order Greenhorn cycle. Within each general lithofacies package, changes in microfacies types reflect variations in magnitude and frequency of storm events, which are inferred to be related to higher-order (e.g. third- to fourth-order) relative sea-level changes. High-frequency relative sea-level cycles during early to middle Turonian within the WIS have been widely documented in a number

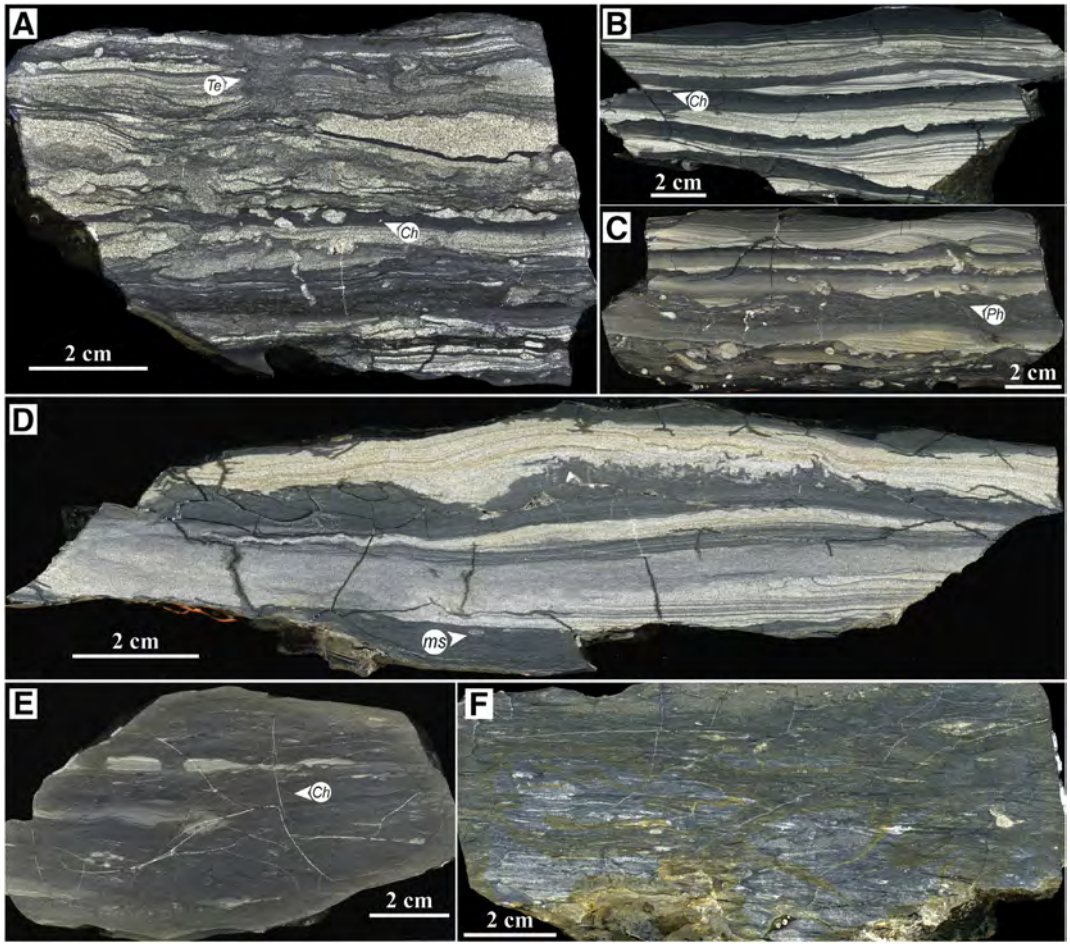


**Fig. 17.** Images of polished slabs of the SSM facies. A) SSMm facies of common disrupted sandstone beds showing wave ripple laminations separated by bioturbated mudstones. B) SSMl facies showing common very fine-grained sandstone beds showing wave ripple and combined-flow ripple laminations separated by rarely bioturbated mudstones. C). SSMm facies of several slightly disrupted sandstone beds showing wave ripple and combined-flow ripple laminations separated by bioturbated mudstones. D) SSMl facies showing silty/sandy wave ripple laminations separated by rarely bioturbated mudstones. Note small loading structure (e.g. flame structure) and angular mud clasts at the base of the topmost wave rippled sandstone bed. E) SSMm facies showing disrupted silty wave ripple laminations. F) SSMh facies. Primary sedimentary features are rarely preserved due to pervasive bioturbation. Samples of A) through F) are from stratigraphic lower to upper locations. Trace-fossil abbreviations include *Te*: *Teichichnus, Ch*: *Chondrites, Ph: Phycosiphon*, ms: "mantle-and-swirl" structure.

of previous studies (e.g. Elder et al., 1994; Leithold, 1994; Sageman et al., 1997; Jarvis et al., 2006; Zhu et al., 2012, etc.).

The dominant depositional environments and depositional processes for the different lithofacies observed in the Tununk Shale are summarized in Fig. 20. Almost the entire Tununk succession was deposited above storm wave base and subject to bedload transport. Storm-induced shore-parallel geostrophic flow and offshore-directed flows likely were the dominant processes that governed the transportation and deposition of mud across and along a storm-dominated shelf. This finding starkly contrasts with prior studies of the Tununk Shale that interpreted it a prodeltaic deposit (Leithold, 1994; Sethi and Leithold, 1997; Leithold and Dean, 1998). If the latter concept were to apply to the Tununk, one would expect to find abundant evidence for surge-type turbidity currents and hyperpycnal flows, because these features are common in the river-dominated prodeltaic mudstones of the directly overlying Ferron Sandstone (Li et al., 2015). Given the great familiarity of the first author with the Ferron mudstones (Li et al., 2015), we can firmly state that neither surge-type turbidity currents and hyperpycnal flows can be documented with any degree of confidence in the Tununk Shale and that it should not be considered a river-dominated prodeltaic deposit. Instead of originating from deltaic progradation, the seaward-dipping clinoforms documented by Leithold (1994) in the Tununk and Tropic Shale are here considered as a stratigraphic expression of storm-induced offshore directed sediment transport that served to expand a shore-parallel mudbank basinwards. The envisioned scenario (Figs. 19 and 20) compares favorably to along-shelf muddy clinoforms that have been documented in a number of modern offshore mud-blankets that were deposited under the influence of strong longshore-currents (e.g. Kuehl et al., 1986; Allison et al., 2000; Cattaneo et al., 2007; Liu et al., 2006; Lazar et al., 2015).

## 6. Conclusion

Detailed analysis of sedimentary and biogenic facies characteristics of the Tununk Shale indicate that it consists of four major lithofacies types: 1) carbonate-bearing, silty and sandy mudstone (CSSM), 2) silt-bearing, calcareous mudstone (SCM), 3) carbonate-bearing, silty mudstone to muddy siltstone (CMS), and 4) non-calcareous, silty and sandy mudstone (SSM). Vertical variations in lithofacies types and sedimentary facies characteristics indicate that the depositional environments recorded by the Tununk succession shifted laterally from distal middle shelf to outer shelf (CSSM to SCM facies), then from outer shelf to inner shelf (SCM to CMS, then to SSM facies), and were largely controlled by the second-order Greenhorn sea-level cycle.

The Tununk Shale is interpreted as an offshore mud blanket on a storm-dominated shelf. Sediment supply for the Tununk Shale mainly came from updrift areas (north of the study area), and was carried southward by longshore-currents. Paleocurrent data provide important

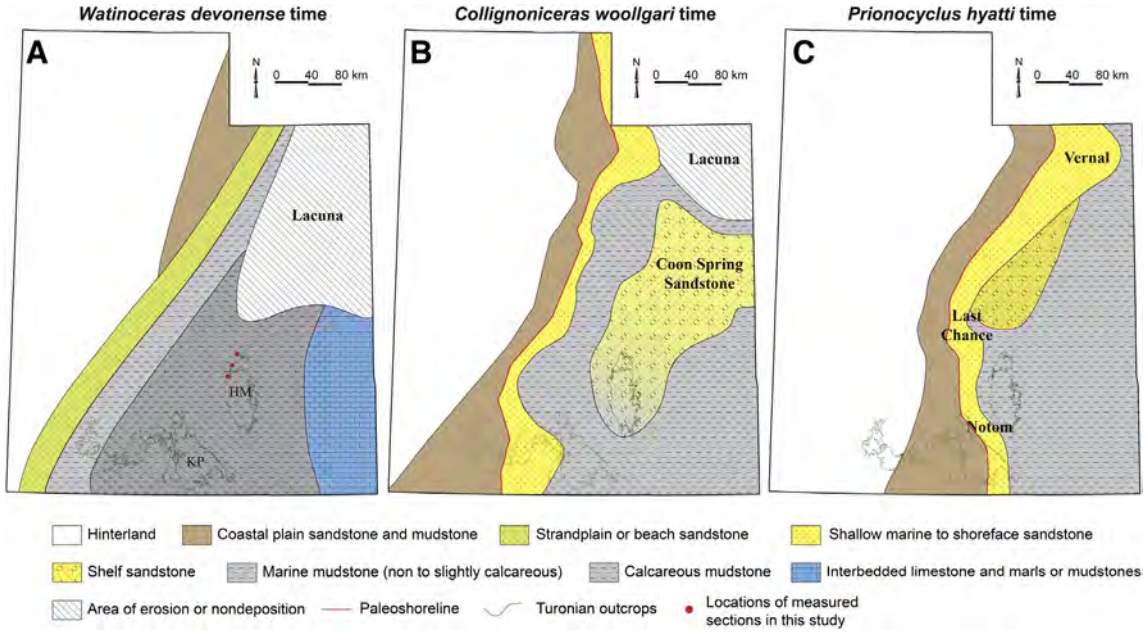


**Fig. 18.** Paleogeographic reconstructions showing the distribution of depositional facies and unconformities. A) Earliest Turonian maximum transgression of the Greenhorn cycle during deposition of the *Watinoceras devonense* zone, about the time that bentonites T4 and T5 accumulated. B) Early middle Turonian during deposition of the *Collignoniceras woollgari* zone, about the time before bentonite T6 accumulated. C) Late middle Turonian during deposition of the *Prionocyclus hyatti* zone, about the time that bentonite T10 accumulated. Paleogeographic maps are reconstructed based mainly on Molenaar (1983), Elder and Kirkland (1994), Gardner (1995), and results from this study.

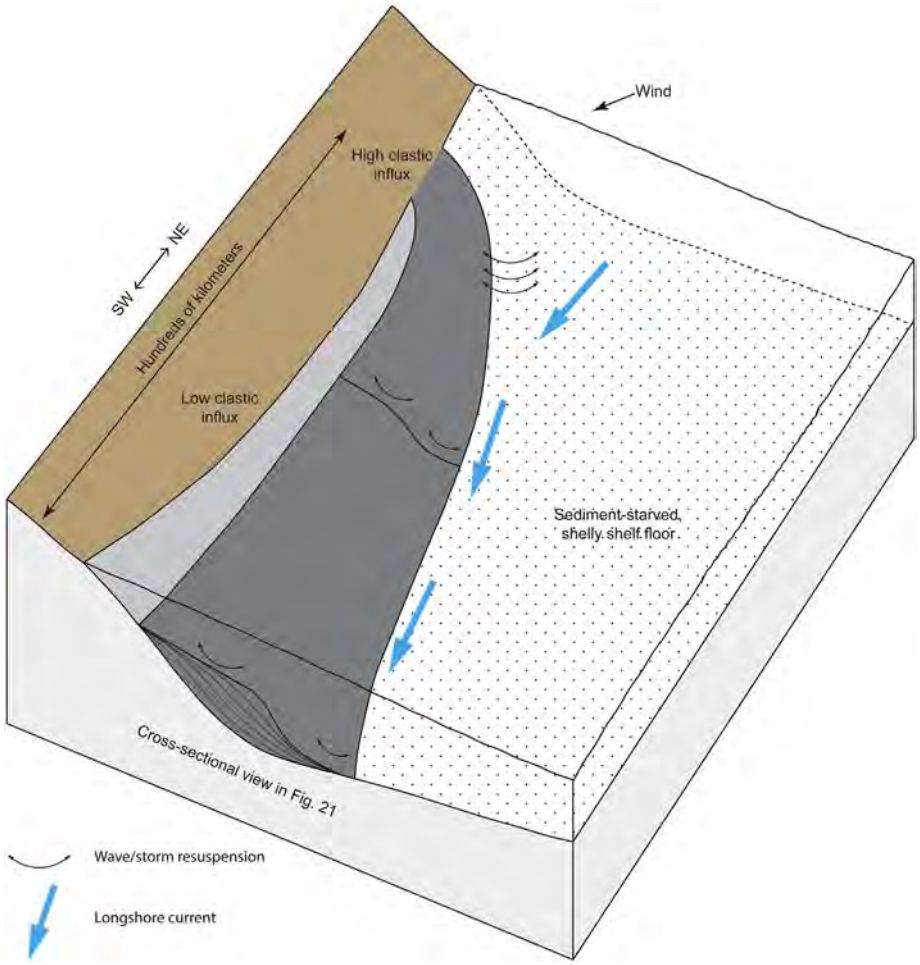


**Fig. 19.** Schematic drawing of the depositional model for the Tununk Shale. Sediments from updrift of study area were deflected by longshore currents and accumulated as an offshore mud blanket a few hundreds of kilometers downdrift. In this case, the updrift area (200–300 km from the study area) was also a shoal area subject to constant wave-storm reworking (Ryer and Lovekin, 1986). The diagram is based on results from this study and various models proposed for comparable mud-rich shelves under strong influence of longshore-currents (Allison et al., 2000; Liu et al., 2006; Cattaneo et al., 2007; Plint, 2014). The presence of mud-dominated clinoforms is suggested by Leithold (1994).

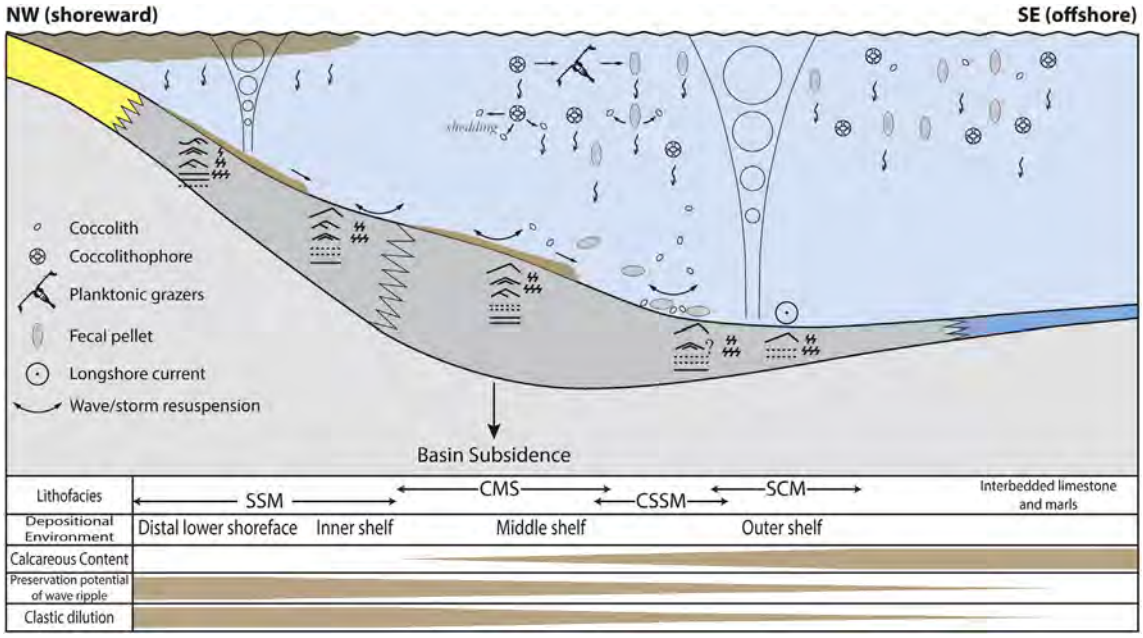


**Fig. 20.** Schematic drawing (cross-sectional view) of the depositional model for the Tununk Shale. See Fig. 6 for facies keys. Sediments from various sources, dominant depositional processes and dominant depositional environments for all lithofacies types observed in the Tununk Shale are summarized. Since deposition of almost the entire Tununk occurred above the average storm wave base for silt, it is important to note that, all sediments probably have undergone multiple cycles of settling and resuspension and significant amount of both along- and across-shelf transport before they were eventually deposited.

constraints for the interpretation of depositional environments of shelf mudstone successions. In the Tununk, dominant shore-parallel sediment transport is recorded in middle to outer-shelf deposits, whereas inner shelf deposits carry the imprint of offshore-directed sediment transport. The comparatively weak but more sustained shore-parallel geostrophic currents play an essential role in carrying sediment along a storm-dominated shelf, whereas stronger but relatively short-lived offshore-directed currents are important for transporting sediment across the shelf.

The facies analysis and depositional model proposed for the Tununk Shale in this study provides a useful interpretative framework for shelf mudstone successions that accumulated away from direct riverine sediment supplies in the storm-dominated WIS as well as elsewhere in the sedimentary record. Because sediment supply to any shelf setting (both allochthonous and autochthonous components) is likely to vary significantly in time and space, caution is advisable when trying to expand the Tununk facies model to other areas within the WIS or other parts of the rock record. Mudstones that may look much the same in outcrop, like the prodeltaic muds of the Ferron and the shelf mudstones of the Tununk (gray and unimpressive), can nonetheless be rather distinct when their sedimentary attributes are examined in detail and reveal a different sedimentary setting and history. From a perspective of multiple case studies, this study as well reinforces the notion that every shale/mudstone deserves its own interpretation.

## Acknowledgement

Comments by Kevin Taylor on an earlier version of the manuscript, as well as suggestions provided by an anonymous reviewer and Journal Editor Brian Jones are greatly appreciated. This research project was supported by the Indiana University Shale Research Consortium (sponsored by Anadarko, Chevron, ConocoPhillips, ExxonMobil, Shell, Statoil, Marathon, Whiting and Wintershall). Fieldwork and analytical supplies were also supported through student research grants awarded to Zhiyang Li by the Geological Society of America, American Association of Petroleum Geologists (Donald A. & Mary O'Nesky Named Grant), SEPM (Society for Sedimentary Geology), and the Indiana University Department of Geological Sciences. Many thanks to Sue Fivecoat and John Reay from the Bureau of Land Management (BLM) at Henry Mountains Field Station for their guidance and help on granting us permits for fieldwork in the study area. We also thank Bei Liu, Britt Rossman, and Matthew Leung for their assistance in the field.

## References

Aigner, T., Reineck, H.E., 1982. Proximality trends in modern storm sands from the Helgoland Bight (North Sea) and their implications for basin analysis. Senckenbergiana Maritima 14, 183–215.
Allison, M.A., Lee, M.T., Ogston, A.S., Aller, R.C., 2000. Origin of Amazon mudbanks along the northeastern coast of South America. Marine Geology 163, 241–256.
Aplin, A.C., Macquaker, J.H.S., 2011. Mudstone diversity: origin and implications for source, seal, and reservoir properties in petroleum systems. AAPG Bulletin 95, 2031–2059.
Armstrong, R.L., 1968. Sevier Orogenic Belt in Nevada and Utah. Geological Society of America Bulletin 79, 429–458.
Barron, E.J., 1989. Severe storms during earth history. Geological Society of America Bulletin 101, 601–612.
Bhattacharya, J.P., MacEachern, J.A., 2009. Hyperpycnal rivers and prodeltaic shelves in the Cretaceous seaway of North America. Journal of Sedimentary Research 79, 184–209.
Bhattacharya, J.P., Tye, R.S., 2004. Searching for modern Ferron analogs and application to subsurface interpretation. In: Chidsey Jr., T.C., Adams, R.D., Morris, T.H. (Eds.), The Fluvial-Deltaic Ferron Sandstone: Regional to Wellbore-Scale Outcrop Analogs Studies and Application to Reservoir Modeling. AAPG Studies in Geology, Tulsa, OK, pp. 39–57.
Birgenheier, L.P., Horton, B., McCauley, A.D., Johnson, C.L., Kennedy, A., 2017. A depositional model for offshore deposits of the lower Blue Gate Member, Mancos Shale, Uinta Basin, Utah, USA. Sedimentology 64, 1402–1438.
Blakey, R.C., 2014. Paleogeography and Paleotectonics of the Western Interior Seaway, Jurassic-Cretaceous of North America. AAPG Search and Discovery Article #30392 pp. 1–72.
Bohacs, K.M., et al., 2005. Production, destruction, and dilution; the many paths to source-rock development. Special Publication - Society for Sedimentary Geology 82, 61–101.
Cattaneo, A., Trincardi, F., Asioli, A., Correggiari, A., 2007. The Western Adriatic shelf clinoform: energy-limited bottomset. Continental Shelf Research 27, 506–525.
Dashtgard, S.E., MacEachern, J.A., 2016. Unburrowed mudstones may record only slightly lowered oxygen conditions in warm, shallow basins. Geology 44, 371–374.
Dashtgard, S.E., Snedden, J.W., MacEachern, J.A., 2015. Unbioturbated sediments on a muddy shelf: hypoxia or simply reduced oxygen saturation? Palaeogeography, Palaeoclimatology, Palaeoecology 425, 128–138.
DeCelles, P.G., 2004. Late Jurassic to Eocene evolution of the Cordilleran thrust belt and foreland basin system, western U.S.A. American Journal of Science 304, 105–168.

Duke, W.L., 1990. Geostrophic circulation or shallow marine turbidity currents? The dilemma of paleoflow patterns in storm-influenced prograding shoreline systems. Journal of Sedimentary Research 60, 870–883.
Ekdale, A., Mason, T., 1988. Characteristic trace-fossil associations in oxygen-poor sedimentary environments. Geology 16, 720–723.
Elder, W.P., Gustason, E.R., Sageman, B.B., 1994. Correlation of basinal carbonate cycles to nearshore parasequences in the Late Cretaceous Greenhorn seaway, Western Interior U.S.A. Geological Society of America Bulletin 106, 892–902.
Elder, W.P., Kirkland, J.I., 1994. Cretaceous Paleogeography of the Southern Western Interior Region. In: Peterson, J.A., Franczyk, K.J. (Eds.), Mesozoic Systems of the Rocky Mountain Region, USA. SEPM (Society for Sedimentary Geology), Rocky Mountain Section, United States, pp. 415–440.
Ericksen, M.C., Slingerland, R.L., 1990. Numerical simulations of tidal and wind-driven circulation in the cretaceous interior seaway of North America. Geological Society of America Bulletin 102, 1499–1516.
Gardner, M.H., 1995. Tectonic and Eustatic Controls on the Stratal Architecture of Mid-Cretaceous Stratigraphic Sequences, Central Western Interior Foreland Basin of North America. In: Dorobek, S.L., Ross, G.M. (Eds.), Stratigraphic Evolution of Foreland Basins. Stratigraphic Evolution of Foreland Basins. SEPM (Society for Sedimentary Geology), pp. 243–282.
Gardner, M.H., Cross, T.A., Caputo, M.V., 1994. Middle Cretaceous paleogeography of Utah. In: Peterson, J.A., Franczyk, K.J. (Eds.), Mesozoic Systems of the Rocky Mountain Region, USA, pp. 471–502.
Haq, B.U., 2014. Cretaceous eustasy revisited. Global and Planetary Change 113, 44–58.
Harazim, D., McIlroy, D., 2015. Mud-rich density-driven flows along an early Ordovician storm-dominated shoreline: implications for shallow-marine facies models. Journal of Sedimentary Research 85, 509–528.
Hattin, D.E., 1975. Petrology and origin of fecal pellets in upper Cretaceous strata of Kansas and Saskatchewan. Journal of Sedimentary Research 45, 686–696.
Hay, W.W., 2008. Evolving ideas about the Cretaceous climate and ocean circulation. Cretaceous Research 29, 725–753.
Honjo, S., 1976. Coccoliths: production, transportation and sedimentation. Marine Micropaleontology 1, 65–79.
Jarvis, I.A.N., Gale, A.S., Jenkyns, H.C., Pearce, M.A., 2006. Secular variation in Late Cretaceous carbon isotopes: a new δ13C carbonate reference curve for the Cenomanian–Campanian (99.6–70.6 Ma). Geological Magazine 143, 561–608.
Kauffman, E.G., 1977. Geological and biological overview: Western Interior Cretaceous basin. Mountain Geologist 14, 75–99.
Kauffman, E.G., 1985. Cretaceous evolution of the Western Interior Basin of the United States. In: Pratt, L.M., Kauffman, E.G., Zelt, F.B. (Eds.), Fine-grained Deposits and Biofacies of the Cretaceous Western Interior Seaway: Evidence of Cyclic Sedimentary Processes, Field Trip Guidebook. Society of Economic Paleontologists and Mineralogists, Tulsa, OK, pp. iv–xiii.
Kauffman, E.G., Caldwell, W.G.E., 1993. The Western Interior Basin in space and time. In: Caldwell, W.G.E., Kauffman, E.G. (Eds.), Evolution of the Western Interior Basin. Geological Association of Canada Special Paper, Toronto, ON, pp. 1–30.
Kineke, G.C., Sternberg, R.W., Trowbridge, J.H., Geyer, W.R., 1996. Fluid-mud processes on the Amazon continental shelf. Continental Shelf Research 16, 667–696.
Knapp, L.J., McMillan, J.M., Harris, N.B., 2017. A depositional model for organic-rich Duvernay Formation mudstones. Sedimentary Geology 347, 160–182.
Komar, P.D., 1998. Beach Processes and Sedimentation. Prentice Hall, Upper Saddle River, N.J (544 pp.).
Kuehl, S.A., DeMaster, D.J., Nittrouer, C.A., 1986. Nature of sediment accumulation on the Amazon continental shelf. Continental Shelf Research 6, 209–225.
Lazar, O.R., Bohacs, K.M., Schieber, J., Macquaker, J.H.S., Demko, T.M., 2015. Mudstone Primer. Lithofacies Variations, Diagnostic Criteria, and Sedimentologic–Stratigraphic Implications at Lamina to Bedset Scale. SEPM (Society for Sedimentary Geology) (205 pp.).
Leckie, D.A., Krystinik, L.F., 1989. Is there evidence for geostrophic currents preserved in the sedimentary record of inner to middle-shelf deposits. Journal of Sedimentary Research 59, 862–870.
Leithold, E.L., 1994. Stratigraphical architecture at the muddy margin of the Cretaceous Western Interior Seaway, southern Utah. Sedimentology 41, 521–542.
Leithold, E.L., Dean, W.E., 1998. Depositional processes and carbon burial on a Turonian prodelta at the margin of the Western Interior Seaway. Concepts in Sedimentology and Paleontology 6, 189–200.
Li, Z., Bhattacharya, J., Schieber, J., 2015. Evaluating along-strike variation using thin-bedded facies analysis, Upper Cretaceous Ferron Notom Delta, Utah. Sedimentology 62, 2060–2089.
Liu, X., Jia, Y., Zheng, J., Wen, M., Shan, H., 2017. An experimental investigation of wave-induced sediment responses in a natural silty seabed: new insights into seabed stratification. Sedimentology 64, 508–529.
Liu, S., Nummedal, D., Liu, L., 2011. Migration of dynamic subsidence across the Late Cretaceous United States Western Interior Basin in response to Farallon plate subduction. Geology 39, 555–558.
Liu, J.P., et al., 2006. Sedimentary features of the Yangtze River-derived along-shelf clinoform deposit in the East China Sea. Continental Shelf Research 26, 2141–2156.
Livaccari, R.F., 1991. Role of crustal thickening and extensional collapse in the tectonic evolution of the Sevier-Laramide orogeny, western United States. Geology 19, 1104–1107.
Lobza, V., Schieber, J., 1999. Biogenic sedimentary structures produced by worms in soupy, soft muds; observations from the Chattanooga Shale (Upper Devonian) and experiments. Journal of Sedimentary Research 69, 1041–1049.
MacEachern, J.A., Bann, K.L., Pemberton, S.G., Gingras, M.K., 2007. The ichnofacies paradigm: high-resolution paleoenvironmental interpretation of the rock record. In: MacEachern, J.A., Bann, K.L., Gingras, M.K., Pemberton, S.G. (Eds.), Applied Ichonology, SEPM Short Course Notes 52. SEPM (Society for Sedimentary Geology), Tulsa, USA, pp. 27–64.
MacQuaker, J.H.S., Gawthorpe, R.L., 1993. Mudstone lithofacies in the Kimmeridge Clay Formation, Wessex Basin, southern England; implications for the origin and controls of the distribution of mudstones. Journal of Sedimentary Research 63, 1129–1143.
Macquaker, J.H.S., Howell, J.K., 1999. Small-scale (<5.0 m) vertical heterogeneity in mudstones: implications for high-resolution stratigraphy in siliciclastic mudstone successions. Journal of the Geological Society 156, 105–112.
Miall, A.D., Catuneanu, O., Vakarelov, B.K., Post, R., 2008. The western interior basin. In: Andrew, D.M. (Ed.), Sedimentary Basins of the World. Elsevier, pp. 329–362 (Chapter 9).
Miller, K.G., et al., 2005. The Phanerozoic record of global sea-level change. Science 310, 1293–1298.
Minoura, K., Osaka, Y., 1992. Sediments and sedimentary processes in Mutsu Bay, Japan: pelletization as the most important mode in depositing argillaceous sediments. Marine Geology 103, 487–502.
Molenaar, C.M., 1983. Major depositional cycles and regional correlations of Upper Cretaceous rocks, southern Colorado Plateau and adjacent areas. Rocky Mountain Paleogeography Symposium 2, 201–224.
Molenaar, C.M., Cobban, W.A., 1991. Middle Cretaceous stratigraphy on the south and east sides of the Uinta Basin, northeastern Utah and northwestern Colorado. p. 1787P.
Nittrouer, C.A., Kuehl, S.A., DeMaster, D.J., Kowsmann, R.O., 1986. The deltaic nature of Amazon shelf sedimentation. Geological Society of America Bulletin 97, 444–458.
Nowell, A.R.M., Jumars, P.A., Eckman, J.E., 1981. Effects of biological activity on the entrainment of marine sediments. Marine Geology 42, 133–153.
Oehmig, R., 1993. Entrainment of planktonic foraminifera: effect of bulk density. Sedimentology 40, 869–877.
Ogg, J.G., Hinnov, L.A., Huang, C., 2012. Chapter 27 — cretaceous. In: Gradstein, F.M., Ogg, J.G., Schmitz, M.D., Ogg, G.M. (Eds.), The Geologic Time Scale. Elsevier, Boston, pp. 793–853.
Owen, G., Moretti, M., 2011. Identifying triggers for liquefaction-induced soft-sediment deformation in sands. Sedimentary Geology 235, 141–147.
Passey, Q.R., Bohacs, K., Esch, W.L., Klimentidis, R., Sinha, S., 2010. From oil-prone source rock to gas-producing shale reservoir — geologic and petrophysical characterization of unconventional shale gas reservoirs. International Oil and Gas Conference and Exhibition in China. Society of Petroleum Engineers, Beijing, China, p. 29.
Peterson, F., Ryder, R.T., Law, B.E., 1980. Stratigraphy, sedimentology, and regional relationships of the Cretaceous System in the Henry Mountains region, Utah. Utah Geological Association Publication 151–170.
Plint, A.G., 2014. Mud dispersal across a Cretaceous prodelta: storm-generated, wave-enhanced sediment gravity flows inferred from mudstone microtexture and microfacies. Sedimentology 61, 609–647.
Potter, P.E., Maynard, J.B., Depetris, P.J., 2005. Mud and mudstones: introduction and overview. Springer-Verlag, Berlin Heidelberg (297 pp.).
Rine, J.M., Ginsburg, R.N., 1985. Depositional facies of a mud shoreface in Suriname, South America; a mud analogue to sandy, shallow-marine deposits. Journal of Sedimentary Research 55, 633–652.
Ryer, T., Lovekin, J., 1986. The Upper Cretaceous Vernal Delta of Utah—depositional or paleotectonic feature. In: Peterson, J.A. (Ed.), Paleotectonics and Sedimentation in the Rocky Mountain Region, United States: Part III. American Association of Petroleum Geologists Memoir, pp. 497–509.
Sageman, B.B., Arthur, M.A., 1994. Early Turonian paleogeographic/paleobathymetric map, Western Interior, U.S. In: C. M., P. J. (Ed.), Mesozoic Systems of the Rocky Mountain Region. Rocky Mountain Section. SEPM Special Publication, United States, pp. 457–470.
Sageman, B.B., Rich, J., Arthur, M.A., Birchfield, G.E., Dean, W.E., 1997. Evidence for Milankovitch periodicities in Cenomanian-Turonian lithologic and geochemical cycles, Western Interior U.S.A. Journal of Sedimentary Research 67, 286–302.
Savrda, C.E., Bottjer, D.J., 1991. Oxygen-related biofacies in marine strata: an overview and update. Geological Society, London, Special Publications 58, 201–219.
Schieber, J., 1989. Facies and origin of shales from the mid-Proterozoic Newland Formation, Belt Basin, Montana, USA. Sedimentology 36, 203–219.
Schieber, J., 1990. Significance of styles of epicontinental shale sedimentation in the Belt basin, Mid-Proterozoic of Montana, U.S.A. Sedimentary Geology 69, 297–312.
Schieber, J., 1999. Distribution and deposition of mudstone facies in the Upper Devonian Sonyea Group of New York. Journal of Sedimentary Research 69, 909–925.
Schieber, J., 2011. Reverse engineering mother nature — shale sedimentology from an experimental perspective. Sedimentary Geology 238, 1–22.
Schieber, J., 2016. Mud re-distribution in epicontinental basins — exploring likely processes. Marine and Petroleum Geology 71, 119–133.
Schieber, J., Southard, J.B., 2009. Bedload transport of mud by floccule ripples—direct observation of ripple migration processes and their implications. Geology 37, 483–486.
Schieber, J., Southard, J., Thaisen, K., 2007. Accretion of mudstone beds from migrating floccule ripples. Science 318, 1760–1763.
Schieber, J., Zimmerle, W., 1998. Introduction and Overview; the History and Promise of Shale Research. In: Schieber, J., Zimmerle, W., Sethi, P.S. (Eds.), Shales and Mudstones (vol. 1): Basin Studies, Sedimentology and Paleontology. Schweizerbart'sche Verlagsbuchhandlung, Stuttgart, pp. 1–10.
Sethi, P.S., Leithold, E.L., 1997. Recurrent depletion of benthic oxygen with 4th-order transgressive maxima in the Cretaceous Western Interior Seaway. Palaeogeography, Palaeoclimatology, Palaeoecology 128, 39–61.
Slingerland, R., Keen, T.R., 1999. Sediment transport in the Western Interior Seaway of North America; predictions from a climate-ocean-sediment model. In: Bergman, K.M., Snedden, J.W. (Eds.), Isolated Shallow Marine Sand Bodies. SEPM Special Publication, pp. 179–190.
Snedden, J.W., Nummedal, D., Amos, A.F., 1988. Storm- and fairweather combined flow on the central Texas continental shelf. Journal of Sedimentary Research 58, 580–595.

Swift, D.J.P., Han, G., Vincent, C.E., 1986. Fluid processes and sea-floor response on a modern storm-dominated shelf; Middle Atlantic Shelf of North America; Part I, The storm-current regime. In: Knight, R.J., McLean, J.R. (Eds.), Shelf Sands and Sandstones. Canadian Society of Petroleum Geologists Memoir, pp. 99–119.

Taylor, A.M., Goldring, R., 1993. Description and analysis of bioturbation and ichnofabric. Journal of the Geological Society of London 150, 141–148.

Traykovski, P., Geyer, W.R., Irish, J.D., Lynch, J.F., 2000. The role of wave-induced density-driven fluid mud flows for cross-shelf transport on the Eel River continental shelf. Continental Shelf Research 20, 2113–2140.

Weimer, R.J., 1984. Relation of unconformities, tectonics, and sea-level changes, Cretaceous of Western Interior, U.S.A. In: Schlee, J.S. (Ed.), Interregional Unconformities and Hydrocarbon Accumulation. American Association of Petroleum Geologists, Tulsa, OK, United States, pp. 7–35.

Williams, C.J., Hesselbo, S.P., Jenkyns, H.C., Morgans-Bell, H.S., 2001. Quartz silt in mudrocks as a key to sequence stratigraphy (Kimmeridge Clay Formation, Late Jurassic, Wessex Basin, UK). Terra Nova 13, 449–455.

Wilson, R.D., Schieber, J., 2014. Muddy Prodeltaic Hyperpycnites in the lower Genesee Group of Central New York, USA: implications for mud transport in Epicontinental seas. Journal of Sedimentary Research 84, 866–874.

Wilson, R.D., Schieber, J., 2015. Sedimentary facies and depositional environment of the middle Devonian Geneseo formation of New York, U.S.A. Journal of Sedimentary Research 85, 1393–1415.

Wilson, R.D., Schieber, J., 2016. The Influence of Primary and Secondary Sedimentary Features on Reservoir Quality: Examples from the Geneseo Formation of New York, U.S.A. In: Olson, T. (Ed.), Imaging Unconventional Reservoir Pore Systems. AAPG Memoir Vol. 112, pp. 167–184.

Wright, L.D., et al., 1988. Marine dispersal and deposition of Yellow River silts by gravity-driven underflows. Nature 332, 629–632.

Yawar, Z., Schieber, J., 2017. On the origin of silt laminae in laminated shales. Sedimentary Geology 360, 22–34.

Yonkee, W.A., Weil, A.B., 2015. Tectonic evolution of the Sevier and Laramide belts within the North American Cordillera orogenic system. Earth-Science Reviews 150, 531–593.

Zelt, F.B., 1985. Natural Gamma-Ray Spectrometry, Lithofacies, and Depositional Environments of Selected Upper Cretaceous Marine Mudrocks, Western United States, Including Tropic Shale and Tununk Member of Mancos Shale, Princeton Univ., Princeton, NJ. Princeton Univ., NJ (USA) (372 pp.).

Zhu, Y., et al., 2012. Milankovitch-scale sequence stratigraphy and stepped forced regressions of the Turonian Ferron Notom deltaic complex, South-Central Utah, U.S.A. Journal of Sedimentary Research 82, 723–746.